
Relativistic Calculations of Atomic Clock

Bijaya Kumar Sahoo

Contents

Introduction	2
Classes of Clocks and Their Status	5
Operational Principles of Atomic Clocks	5
Other Possible Candidates	9
Typical Systematics	10
Instrumental Effects	11
External Effects	12
Relativistic Many-Body Methods	20
General Approach	21
Random-Phase Approximation (RPA)	28
Demonstration of Few Theoretical Results	29
A_{hf} -Constants and g_J -Factors	29
Static Polarizabilities (In Au)	31
Quadrupole Moments	33
Clocks for Fundamental Physics	38
Summary	42
References	42

Abstract

A pedagogic introduction to the atomic clock physics, mainly from a theoretical viewpoint, is presented, and the need for sophisticated relativistic many-body methods for their studies is emphasized. Few general aspects on the working principles of atomic clocks, their necessities in the daily life as well as for the fundamental sciences, and their present status are outlined. Special attention has been paid to keep the discussion at the graduate course level. Basic physics related to major systematics in an atomic system exposed to external

B.K. Sahoo (✉)

Theoretical Physics Division, Physical Research Laboratory (PRL), Ahmedabad, Gujarat, India
e-mail: bijaya@prl.res.in

electromagnetic fields and theoretical approaches for their accurate estimations for the atomic clock frequency measurements are highlighted. In this context, we discuss the roles of many-body methods to evaluate Stark, Zeeman, quadrupole, and multipolar blackbody radiation shifts and to search for magic wavelengths in the atomic systems. A few examples are given to show usefulness of theoretical perception for scrutinizing suitability of a candidate as an atomic clock a priori to performing measurement. Since the modern atomic clocks offer most precise measurements of the atomic transition frequencies, they are also used as tools for probing both temporal and spatial variation of many fundamental physical constants at the low-energy scale. The requirement of relativistic many-body methods to yield information on the temporal variation of fine-structure constant from the atomic clock studies is demonstrated. Several theoretical methods, capable of calculating atomic properties very accurately, are prescribed to facilitate better comprehension to the subject.

Keywords

Atomic clock • BBR shift (black-body radiation shift) • Configuration interaction (CI) • Coupled-cluster (CC) • Doppler effect • Fine structure constant • Frequency standard • Instability • Linewidth • Magic wavelengths • Micromotion • Microwave clock • Optical clock • Quadrupole shift • Quality factor • Random phase approximation (RPA) • Reproducibility • Secular motion • Signal-to-noise ratio • Stark shift • Zeeman shift

Introduction

An **atomic clock** is a device that uses resonance frequency of an electromagnetic transition between two energy levels in an atomic system as frequency standard to count ticks between two consecutive seconds. More than 50 years ago, Essen and Parry had proposed for the first time to use transition frequency between the hyperfine sublevels of the ground state in Cs atom to define unit of time. Today, this frequency is measured up to 9,192,631,770 oscillations per unit of time (known as second) and is conceded as primary **frequency standard**. This sort of accuracy is several orders higher than the accuracies of a typically used quartz clock in the daily life activities. The guiding cause for accrediting atomic transition frequencies as the time or frequency standards lies in their origin as they are the consequences of the fundamental interactions between the elementary particles; their values must remain the same irrespective of their locations or time of measurements. A selection criterion for a particular transition to be considered for this purpose depends mainly on three critical factors: a transition frequency that can be probed by a short-term stable local oscillator, the availability of a suitable frequency-counting mechanism, and a weak forbidden transition having intrinsic narrow natural **linewidth**. Broadly, atomic clocks are classified into either active or passive depending on whether the frequency standard is derived directly from the electromagnetic radiation or it is probed by an electromagnetic radiation of an external oscillator.

One of the quantities that signifies a better frequency standard is the **quality factor** (Q), defined as $Q = \frac{\nu}{\delta\nu}$ where ν and $\delta\nu$ are the transition frequency and linewidth of the transition, respectively. The ultimate objective would be to search for an atomic clock with Q -factor as large as possible. The accuracy of an atomic clock cannot be, in fact, defined uniquely. In practice, it quantifies either the offset of a frequency standard from its normal operating frequency or how well the frequency of the device can be related to the standard international (SI) unit of frequency. We shall return back to the estimation of uncertainties in the determination of the offset from its original value of the frequency in an atomic clock later. Another important aspect that also needs to be looked into before accepting candidates for atomic clocks is their **instability** and **reproducibility** limitations. Stability (as opposed to instability) is a measure of variability of the frequency standard over a specified period of time. Gauging this quantity requires a suitable reference standard having either lower or equally compatible stability with the considered atomic clock. All the three factors (reproducibility, accuracy, and instability) of an atomic frequency standard depend on the sensitivity of the reference frequency to the environmental perturbations and to the extent within which these perturbations can be controlled. The stability of the frequency standard is generally characterized by either two-sample or Allan variance given by [2]

$$\sigma_y^2(\tau) = \left\langle \frac{1}{2} \sum_k (\bar{y}_k - \bar{y}_{k+1})^2 \right\rangle, \quad (1)$$

where \bar{y}_k is the mean fractional deviation frequency measured at time t_k with an interval dt_k from its nominal operating frequency ν_0 over the averaging period τ and reads

$$\bar{y}_k = \frac{1}{\tau} \int_{t_k}^{t_k+\tau} y(t_k) dt_k = \frac{1}{\tau} \int_{t_k}^{t_k+\tau} \frac{\nu(t_k) - \nu_0}{\nu_0} dt_k. \quad (2)$$

For better statistical accuracy, the average value needs to be evaluated by integrating over a large period of time τ . The final deviation is determined as the square root of the variance.

The present primary Cs clock is a **microwave clock**; however, most of the modern clocks are preferred to operate in the optical frequencies. The **optical clocks** operate at frequencies about five orders of magnitude higher than the Cs clock. The local reference in an optical clock is generally a narrow linewidth laser that is stabilized to a narrow optical atomic reference transition. Candidates chosen for the optical clocks can be grouped into two major classes: neutral atoms trapped and cooled using magnetic optical traps (MOT) and a single singly and multiply charged ion trapped using the Paul-type trap. The real state of the art for considering optical transitions as the frequency standards lies in their stabilities and to the precisions at which the uncertainties associated with their measurements can be elucidated. Instability in the fractional frequency shift due to the quantum fluctuations in an atomic absorption signal can be estimated by

$$\sigma_y(\tau) = \frac{n}{Q(S/N)} \tau^{1/2}, \quad (3)$$

where S/N is the **signal-to-noise ratio** for a 1 Hz detection bandwidth and ν value depends on the shape of the atomic resonance line and the method used to determine its central frequency. From the above expression, it can be understood that stability is a measure of the precision within which a given quantity can be measured and is usually stated as a function of averaging time. Owing to this fact, very significant reduction in the instability is gained in the optical clocks. The reduction factors depend exactly on the signal-to-noise ratio at which the atomic absorption signal is observed and proportional to $N^{1/2}$, where N is the number of atoms detected in the measurement process. Thus, the atomic clocks based on the optical lattices have relatively large stability compared with the microwave clocks as well as from a single ionized optical clock. The other concern in setting up an atomic clock is the uncertainties in the systematics, arising due to the sensitivity of an experiment to the environmental perturbations, which can shift the measured frequency from its unperturbed natural atomic frequency. It is, indeed, indispensable to expect suppressed systematics for an ideal frequency standard. Thus, it is imperative to understand all the physical processes happening surrounding the experiments and enable to estimate their systematics rigorously. It is also important that clock frequency can be reproducible irrespective of the location and time of an experiment. Contemplating both reproducibility and sensitivity to the environmental perturbations, there seems to be strong competition between the optical clocks based on the cold neutral atoms trapped in the optical lattices and a singly charged ion trapped using the Paul trap to replace the Cs microwave clock to become the next-generation primary frequency standard. In this scenario it is very much useful to have comprehensive understanding about the present status of different atomic clocks that are under consideration in different laboratories around the world and the roles of various environmental perturbations that are accountable for limiting the accuracies of the atomic clocks.

Among other prominent applications, atomic clocks are the essential components of the global positioning system (GPS). Each GPS satellite contains multiple atomic clocks. GPS receivers decode detected signals by synchronizing each receiver to the atomic clocks. In this process, it provides very precise time to an observed GPS signal and helps in finding out position and time of an object. It provides us the time to within 100 billionths of a second. Atomic clocks are also employed for synchronizing various signals from different instruments to carry out high-precision measurements. This is very important to differentiate tiny signatures that are observed in the high-resolution instruments like the measurements that are carried out using high-energy-based accelerators in the particle physics to probe any possible subtle effects governed by the fundamental interactions. In addition, these clocks are of immense use in the radio astronomy, telecommunications, meteorology, military services, etc. Besides, there are of intense investigations carried out for studying fundamental sciences directly using atomic clock signals. At the end of this chapter, a special section is devoted describing principles of probing variation in fundamental constants, especially the **fine-structure constant** α_e , using the atomic clock studies.

The main objective in this chapter would be to demonstrate the requirement of relativistic many-body methods in the context of studying physics related to atomic clocks. One may wonder how theoretical calculations in the considered atomic systems for the frequency standards could be useful at the standpoint where everything seems to be very precise. Note that most of the clock candidates are heavy atomic systems and performing ultrahigh precision calculations in these systems is insurmountable. Although the systematics of atomic clocks themselves are small but the physical quantities of atomic systems associated with these systematics are essentially large enough to be calculated accurately. All the physical quantities measured in the atomic clock experiments are undoubtedly very precise; hence, these observed results can also act as benchmarks for testing the capability of a (relativistic) many-body method to reproduce the experimentally measured quantities. Indeed, it requires powerful many-body methods for theoretical studies that are capable of taking care both the relativistic and electron correlation effects adequately. It is also worth mentioning that appropriateness of a candidate for an atomic clock can be prejudged from the knowledge of the calculated quantities a priori to actual measurement. Thus, it would be vital to understand differences and similarities among the theoretical methods used for the calculations to validate their reported results. In this regard, an attempt is made to formulate various many-body methods with the common starting point (reference state).

Classes of Clocks and Their Status

Operational Principles of Atomic Clocks

The advent of frequency comb is one of the major discoveries in the last century. It helps in stabilizing mode-locked femtosecond lasers to a very high degree and acts as a frequency divider connecting with frequencies of the entire range of the optical spectra. In fact, this can compare two atomic clocks hand in hand even falling under far apart range like optical to microwave frequencies. Frequency combs are used as common references to provide better stabilities to the optical clocks, which also helps to define accuracies of atomic clocks in an elegant manner. Confining atoms or ions for optical clocks in small regions under ultrahigh vacuum makes them well isolated from the environmental perturbations, and they produce narrow linewidths for the transitions as per the obligation. However, thermal motions of atoms and ions trapped using the electromagnetic fields in the optical clocks put tremendous challenges to reduce systematics during the clock frequency measurements. Also, operating the clocks at room temperature can give rise to a velocity distribution for the atoms causing Doppler shifts. In the Paul traps, the residual thermal motion and the **micromotion** of the ions can produce second-order Doppler shifts. Various sub-Doppler techniques have been invented recently to resolve atomic resonances much narrower than those of the Doppler distributions to eliminate **Doppler effects**. The advanced cooling and trapping techniques that make use of an array of lasers and external electric and/or magnetic fields are able to reduce these effects acutely. Techniques like the use of ultralow expansion glasses to measure quantum fluctuations on a fast time scale with a high S/N ratio have also been developed

to minimize many systematics. Depending on the choices of the candidates, special skills are being exploited to overcome these challenges. For example, it is argued that by confining microwave hyperfine transitions in the ground states of Cs and Rb atoms in an optical lattice generated by a circularly polarized laser field and by applying an external magnetic field with appropriately chosen direction may cancel out the dynamic Stark frequency shifts [3]. This may improve the accuracy in the frequency of Cs clock as in this case the clock transition is insensitive to the strengths of both the laser and external magnetic fields.

On the basis of ionic charges, general characteristics of optical clocks distinguish from each other and few of their working principles are discussed below case-wise by highlighting their advantages and drawbacks in constraining accuracies of the clocks.

Optical Lattice Clocks

Optical lattice clocks employ neutral atoms trapped in a specially engineered standing-wave laser fields, termed as magic trapping that uses magnetic optical trap (MOT) to form a lattice kind of potential structure with regular spacing. Its main advantage is that since the interactions between the neutral atoms are fairly short ranged, millions of atoms can be trapped and interrogated simultaneously. It extraordinarily improvises the stability of the clock owing to \sqrt{N} -factor offered by N -number of ensemble atoms trapped in the system. In this case, individual energy levels of a clock transition may be perturbed very strongly by the trapping fields; however, at the magic conditions both the clock levels are shifted almost identically. As a result, magic optical trapping potentials for clock transitions are defined for specific tailored trapping fields in which differential shifts of the clock transitions consequently vanish. The effects of optical laser trapping fields on energy levels are quantified using the ac **Stark shifts** that can be expressed in terms of the dynamic polarizabilities of the states and strengths of the applied electric fields. Even when the electric field oscillates, as in lasers, the differential Stark shift of a transition between two energy levels remains time independent. In this approach very narrow hyperfine-induced transitions, such as the $ns^2\ ^1S_0 \rightarrow nsnp\ ^3P_0$ transitions (n being the principal quantum number of the ground state) in the fermionic stable isotopes of alkaline earth elements (Be, Mg, Ca, Sr, Ba, and Ra atoms), can be exercised to make felicitous frequency standards. The analogous transitions from the rare-gas Zn, Cd, Hg, and Yb atoms can also fulfill the same errand. In fact, the atomic $ns^2\ ^1S_0 \rightarrow nsnp\ ^3P_0$ transitions of the corresponding bosonic stable isotopes are strictly forbidden by the angular momentum and parity selection rules. Applying small external magnetic fields, the excited $nsnp\ ^3P_0$ states of these transitions can mix with their almost-degenerate fine-structure $nsnp\ ^3P_1$ states. Under this condition $nsnp\ ^3P_0$ the states can gain finite lifetimes and can be used as the interrogation time when the $ns^2\ ^1S_0 \rightarrow nsnp\ ^3P_0$ transitions are considered for frequency standards. These transitions thrive as perfect atomic clocks because of their contrived linewidths which can be manipulated to yield optimum stability by selecting the strengths of the applied magnetic fields. Thus far the most stable clock frequency of the above hyperfine-induced transition in ^{87}Sr has been measured

Table 1 Comparative analysis of important clock properties among few leading optical clocks

System	Clock transition	λ (in nm)	Natural linewidth (in Hz)	Observed linewidth (in Hz)	Fractional uncertainty (in $\times 10^{-15}$)	Instability (in $10^{-15} \tau^{-1/2}$)
Atoms						
^{40}Ca	$^1S_0 \leftrightarrow ^3P_1$	657	375.0	250.0	4.2	1.8
^{87}Sr	$^1S_0 \leftrightarrow ^3P_0$	698	0.001	0.5	0.006	0.4
^{171}Yb	$^1S_0 \leftrightarrow ^3P_0$	578	0.01	1.0	0.36	1.5
^{174}Yb	$^1S_0 \leftrightarrow ^3P_0$	578	0.0	4.0	1.5	5.5
^{199}Hg	$^1S_0 \leftrightarrow ^3P_0$	266	0.1	11.0	5,000	5.4
^{201}Hg	$^1S_0 \leftrightarrow ^3P_0$	266	0.1	11.0	5,000	5.4
Ions						
$^{27}\text{Al}^+$	$^1S_0 \leftrightarrow ^3P_0$	267	0.008	2.7	0.0086	0.6
$^{40}\text{Ca}^+$	$S_{1/2} \leftrightarrow D_{5/2}$	729	0.2	30.0	2.4	
$^{88}\text{Sr}^+$	$S_{1/2} \leftrightarrow D_{5/2}$	674	0.4	5.0	0.021	1.1
$^{171}\text{Yb}^+$	$S_{1/2} \leftrightarrow D_{3/2}$	436	3.1	10.0	0.45	
	$S_{1/2} \leftrightarrow F_{7/2}$	467	10^{-9}	7.0	0.071	
$^{199}\text{Hg}^+$	$S_{1/2} \leftrightarrow D_{5/2}$	282	1.7	6.7	0.019	

within 3×10^{-17} fractional uncertainty and a stability of better than $0.4 \times 10^{-15} \tau^{-1/2}$ [2, 4, 5].

A synchronous frequency comparison has been demonstrated of two optical lattice clocks using ^{87}Sr and ^{88}Sr atoms with the Allan standard deviation 1×10^{-17} in an averaging time of 1,600 s [2, 4, 5]. Similarly in ^{174}Yb , magnetically induced transition has been observed for a width of 5 Hz with the reported fractional uncertainty 1.7×10^{-15} and a stability better than $5.5 \times 10^{-16} \tau^{-1/2}$ [2, 4, 5]. Particularly, clock transitions from ^{199}Hg and ^{201}Hg exhibit small blackbody radiation shifts (**BBR shifts**), and their clock frequencies are observed within the fractional uncertainties to 5×10^{-12} [2, 4, 5]. In Table 1, we compare many pivotal properties of few leading atomic clocks accumulating from the review articles [2, 4, 5] to enliven about their adequacies and to explore about other better possible ways to boost their further advancements.

Singly Charged Ions

Although it appears as if use of a single singly charged trapped ion is a drawback in view of instability for an optical clock, but owing to developed competent principles to keep the ions isolated from the environmental perturbations makes them expedient contenders for the atomic clocks. Narrow transitions in several ions have been identified which are potentially pertinent for the optical frequency standards. Each of these ions has its own advantage and disadvantage in terms of clock transition parameters and intrinsic sensitivity to the environmental perturbations as well as in their technical complexities for running the corresponding experiments. The typical working scheme of a singly charged ion, presumed to be suitable for optical frequency standard, comprises a strong allowed transition for the laser cooling and a weak forbidden transition as the frequency reference.

The frequency is readily observed by detecting the resonance fluorescence from the strong cooling transition; however, detecting absorption of individual photon at the frequency of narrow reference transition is, in practice, not an easy affair. This is achieved by an electron shelving technique, whereby quantum jump in the cooling laser fluorescence signal is observed by driving the ion to the upper state of the reference transition by the clock laser. This trick empowers the narrow reference transition to be detected within incredible efficiency. The line profile of a clock transition can be built up by measuring quantum jump probability as a function of the probe laser frequency. The probe laser can be stabilized to the reference transition by repeatedly stepping its frequency back and forth between two estimated half-maximum intensity points of the resonance curve and monitoring the quantum jump rate imbalance between these two points. This quantum jump imbalance can provide a frequency discriminant from which a correcting steer to the frequency of the probe laser can be derived. Some of the prominent and routinely used ions are $^{27}\text{Al}^+$, $^{40}\text{Ca}^+$, $^{43}\text{Ca}^+$, $^{87}\text{Sr}^+$, $^{88}\text{Sr}^+$, $^{115}\text{In}^+$, $^{171}\text{Yb}^+$, $^{173}\text{Yb}^+$, $^{199}\text{Hg}^+$, and $^{201}\text{Hg}^+$ in which a lot of developments are carried out toward frequency standards. Few important key parameters of these standards are already compared in Table 1. Clock transitions from the alkaline earth ions, Yb^+ and Hg^+ , involve ground S-states and one of the metastable $^2\text{D}_{3/2,5/2}$ states that lie below the $^2\text{P}_{1/2,3/2}$ states. Therefore, these D-states decay to their ground S-states via the electric-quadrupole transitions with natural linewidths in the range of 0.2–3 Hz, while the $\text{P}_{1/2}$ to $\text{S}_{1/2}$ transitions are used for cooling the ions. The highest observed Q -factor 1.6×10^{14} is achieved for $^{199}\text{Hg}^+$ with linewidth of 6.7 Hz [2, 4, 5]. The other important set of ions are $^{27}\text{Al}^+$ and $^{115}\text{In}^+$ having electronic configurations similar to the alkaline earth elements; their $ns^2 \ ^1\text{S}_0 \rightarrow nsnp \ ^3\text{P}_0$ transitions are analogous to the previously discussed lattice clock transitions, which are also considered for frequency standards. Mixing of the $nsn \ ^3\text{P}_0$ states with the $nsnp \ ^3\text{P}_1$ and $nsnp \ ^1\text{P}_1$ states due to their hyperfine interactions allows to measure the transition frequencies of the above transitions in sufficiently finite time. These transitions are ideal for the frequency standards because of their longer stability and for exhibiting low systematic frequency shifts. A direct comparison of measurement between the $^{199}\text{Hg}^+$ and $^{27}\text{Al}^+$ frequency standards has been carried out with a relative uncertainty in their ratio as 5.2×10^{-17} for the total systematic uncertainties 1.9×10^{-17} and 2.3×10^{-17} in Hg^+ and Al^+ , respectively, and for the frequency stability $4 \times 10^{-15} \tau^{-1/2}$ [4, 5]. Further clock frequency of the $^1\text{S}_0 \leftrightarrow ^3\text{P}_0$ transition in the same group Al^+ ion is measured independently trapping with the Mg^+ and Be^+ ions with the achievement of a relative statistical measurement uncertainty of 7.0×10^{-18} improved with the Mg^+ ion for a relative stability of $2.8 \times 10^{-15} \tau^{-1/2}$ and a fractional frequency difference of 1.8×10^{-17} [2, 4, 5]. In other set of experiments, a frequency instability of $9 \times 10^{-15} \tau^{-1/2}$ with reproducibility at the 6×10^{-16} level for the $[4f^{14}]6s \ ^1\text{S}_0 \rightarrow [4f^{14}]5d \ ^2\text{D}_{3/2}$ clock transition in $^{171}\text{Yb}^+$ [2, 4, 5] and absolute frequency difference between the ^{87}Sr and $^{87}\text{Sr}^+$ clocks up to 2.8×10^{-17} [4, 5] have been accomplished. In a categorically different experiment with the octopole transition $[4f^{14}]6s \ ^1\text{S}_0 \rightarrow [4f^{13}]6S^2 \ ^2\text{F}_{7/2}$ in $^{171}\text{Yb}^+$, which is insensitive to the field-induced transitions and for possessing very long lifetime of its metastable

excited state (about 6 years), a fractional uncertainty of 7.1×10^{-17} with quantum projection noise $\sigma_y(5,000 s) = 6 \times 10^{-17}$ has been reported [4, 5]. Among many other proposed ions, theoretical analysis also projects that both the $S \leftrightarrow D_{3/2,5/2}$ transitions in the Ba^+ and Ra^+ ions are also capable for realizing them as very high accurate frequency standards [6–8].

Highly Charged Ions

There have been recent proposals [9] to consider single but a highly charged ion as new atomic clock for bespeaking only minuscule systematics encountered by such ions. This owes to their strikingly shrunk orbitals which get least affected by the external perturbations. Since the radiative transition matrix elements are proportional to power expression of the atomic radius, coupling of atomic states with the external fields scales down for increasing charge of an ion. This is an obviously favorable condition for becoming an atomic clock and is the key factor why it is believed that the highly charged ions can be the unrivaled clocks. In principle, highly charged ions can be loaded in the ion traps by employing sympathetic cooling techniques along with another ion species, say Be^+ ions [9]. At sufficiently low temperatures the rates of undesirable charge-exchange processes between two ionic species become negligible. In this scheme, long-range elastic Coulomb collisions with continually laser-cooled Be^+ ions can drive these highly charged ions with temperature down to mK. It is possible to co-trap heavy highly charged ions with relatively light ions of low ionic charge depending upon the ratio of ion charge to its mass. In fact heavier cooling species like Mg^+ can also be used instead of Be^+ to improvise mass matching, hence the cooling efficiency. It is found that the transitions among the fine-structure levels of the ground state in ions having $[4d^{10}]f^{12}$ electronic configuration, e.g., $[4d^{10}]f^{12} {}^3H_6 \rightarrow [4d^{10}]f^{12} {}^3F_4$ transition, are the most felicitous ions for constructing such kind of frequency standards [9].

The feasibility of using magnetic-dipole (M1)-induced hyperfine transitions in the highly charged ions has also been looked into for possible atomic clocks with exceptional accuracy on the basis of anticipated negligibly small blackbody radiation (BBR), quadratic **Zeeman**, ac Stark, and **quadrupole** shifts in these ions [10]. The advantage of these clocks over other hyperfine clock transitions is that wavelengths of the corresponding transitions fall within the optical domain, while most of the other considered ground state-based hyperfine clock transitions lie in the microwave spectral region.

Other Possible Candidates

In spite that there is a less scope to discuss elaborately and connect the need of relativistic calculations at present, a brief discussion on proposed prospective nuclear and molecular clocks is presented for the sake of completeness and to give a broad outlook on this topic to the general readers.

Nuclear Clock

Nuclear systems, where the most common three fundamental interactions strongly interplay each other, are very interesting from the point of view of studying many fundamental sciences; however, their spectroscopy was not yet explored for metrology purposes owing to strenuous procedure to keep bare atomic nucleus isolated. In 2003, Peik and Tamm came up with an idea [11] proposing to use nuclear transition in the $^{229}\text{Th}^{3+}$ ion for the frequency standard. Radioactive ^{229}Th nucleus has an isomeric nuclear state at the unusually low excitation energy of 3.5 ± 1.0 eV above the ground state and its lifetime is about two to four times smaller than the half-life of its nucleus. This energy is comparable with the excitation energies of outer electrons in the atomic shell of $^{229}\text{Th}^{3+}$. The corresponding transition wavelength lies in the range of available tunable laser sources using which its frequency can be measured very precisely. However, the measurement of the corresponding frequency may encounter two important limitations. The under-considered transition will experience a significant second-order differential Zeeman shift ($\sim 70 \text{ kHz}/mT^2$), and their electric-quadrupole transitions could restrict the clock linewidths to ~ 1 Hz. It has been demonstrated that a pair of stretched hyperfine states within the $5F_{5/2}$ electronic ground level of both the nuclear ground and isomeric manifolds in $^{229}\text{Th}^{3+}$ could provide a clock linewidth of $\leq 100 \mu\text{Hz}$ and can offer unprecedented systematic shifts [12].

Molecular Clock

It is also proposed fairly recently by Schiller et al. [13] after carrying out calculations of external-field shift coefficients and analyzing at least 11 systematic effects in the one-electron molecular H^{+2} and HD^+ ions that frequency measurements in their ro-vibrational transitions may reach up to 2×10^{-17} uncertainty at the room temperature. They also argued that by considering measurement of composite $M + 1$ transitions (M being the number of systematic effects to be canceled) in different wavelength ranges, one can reduce the external-field effects. Following this proposal, Karr was quick to estimate light shifts induced by the probe laser using his calculated values of transition amplitudes, differential dynamic polarizability, hyperfine-structure constants, and clock interrogation times for the states accessible by the two-photon and quadrupole transitions [14]. From the estimation of quadrupole and Zeeman shifts, he showed that light shift is the main limiting factor in the case of two-photon transitions for both the H^{+2} and HD^+ ions and gave an estimated accuracy level close to 5×10^{-16} in the best possible case. However, he suggested that quadrupole transitions could be better as promising clock transitions with the estimated accuracies reaching beyond 1×10^{-16} .

Typical Systematics

Systematics in the frequency standard measurements are categorically of two types. One of them is due to the construction of the instruments (defined as instrumental systematics), while the other one is subjected to expose the systems

to the external or stray electromagnetic fields (defined as external systematics). Generally, instrumental systematics depend on size, shape and construction of the mechanical devices, while systematics caused by the external forces are guided by the atomic state properties and the strengths of the applied fields. Thus, the latter systematics can be controlled by suitably choosing clock transitions and by optimizing strengths of the electromagnetic fields. In the theoretical calculation prospects, atomic properties that are relevant to the external systematics are of immense interest. A brief discussion on both types of systematics is outlined below.

Instrumental Effects

With atomic clocks operating in the optical lattices, millions of atoms are trapped and interrogated simultaneously. The mechanism of trapping atoms with lasers brings a seemingly insurmountable challenge, and most of their instrumental systematics depend on the configurations of the devices. One of the major systematics is due to the Doppler's shifts which are reduced by the Doppler cooling technique given by Hänsch and Schawlow. In contrast, issues related with ion clocks are technically different. It follows from Maxwell's equations that it is not possible to trap a charged particle using three-dimensional potential well; however, they can be confined in the Penning and Paul traps. In Penning traps, three-dimensional confinement is achieved by the combination of a strong static magnetic field and a quadrupolar electrostatic field. Since trapped ions are strongly perturbed by the applied fields in the Penning traps, such traps are incompatible for the optical frequency standards, and hence, the Paul traps are commonly used for clocks. In these traps the quadrupole potential seen by the ions is

$$\phi(r, z, t) = (Q_{dc} + Q_{ac} \cos \Omega t)(r^2 - 2z^2), \quad (4)$$

with the dc and ac components of the potential Q_{dc} and Q_{ac} , respectively, for the angular frequency Ω (known as micromotion frequency). Appropriately selecting values of Q_{dc} , Q_{ac} , and Ω , motions of the ions can be stabilized in both the radial and axial directions. Under these conditions the motions of the trapped ions can be separated into two parts, a driven oscillatory motion at the trap drive frequency (micromotion) and a slower motion associated with the time-averaged confining potential (**secular motion**). The characteristic frequency of the secular motion is an order of magnitude smaller than Ω . The typical depth of the Paul traps is of the order of 10 eV, which is sufficient enough to capture ions created by the electron impact ionization or photo-ionization of neutral atoms emitted from a hot oven. The ions are laser cooled within the traps and confined to a region with dimensions less than the wavelengths of the light used to probe the reference transitions of the optical clocks. This is referred to as Lamb–Dicke regime, where the first-order Doppler effect is completely eliminated. The micromotion of the ion leads to amplitude modulation of the cooling laser fluorescence via the Doppler effect and allows to be monitored using radio-frequency photon-correlation techniques. In this approach, micromotion

is minimized by applying small dc voltages to additional compensation electrodes and also the second-order Doppler shift is greatly reduced by confining the ion tightly to the center of the trap. It is also necessary to operate the trap under ultrahigh vacuum condition to reduce the collisional perturbations.

External Effects

In order to determine the overall uncertainty budgets for the optical frequency standards with trapped atomic systems, it is a requisite to consider the effects of environmental perturbations such as magnetic, trapping electric, and applied-light fields on the trapped atoms or ions. External magnetic fields interact with the magnetic moments of the atomic states leading to linear Zeeman shifts of the atomic transition frequencies. In cases like clock transitions in the odd isotopes of alkali-like ions, which have half-integral nuclear spin I , it is possible to select a magnetic field-independent $m_F = 0 \leftrightarrow m_F = 0$ component of the clock transition. These transitions can still experience second-order Zeeman shifts; however, they can be controlled at an acceptable precision level by operating the frequency standard in a low magnetic field of around 1 mT . In addition, the quadrupole shifts due to the interaction between the electric-field gradient and the atomic electric-quadrupole moments can also be eliminated by averaging out the shifts to the transition frequency over three mutually orthogonal magnetic-field orientations. Nonetheless, knowing the functional form of the perturbation due to the quadrupole shift is still very useful for conducting the experiment facily. Stark shifts of the clock transition frequency in a trapped atom or ion can arise in a variety of ways. Firstly, the micromotion and the thermal motion of the atom or ion within the trap cause it to experience a nonzero root mean square value of the electric field. The magnitude and stability of this field depend on the stray charges present within the trap. With careful micromotion compensation, it should be possible to reduce these effects to few parts in 10^{18} level. Secondly, there will be a blackbody Stark shift due to the temperature of the apparatus surrounding the atom or ion. All the cooling, repumper, and clearing-out laser beams can be switched off, while the clock transition is being probed in order to minimize the surrounding effects, but the probe laser light has to be on throughout the experimentation. Thus, the Stark shifts can still be present, but they can be reduced by manipulating intensities required to drive the clock transitions. However, for the kind of laser linewidths achieved these days in the clock frequency measurements, high laser intensity is required to drive these transitions at reasonable rates. Hence, the transition frequencies are measured as functions of laser power and extrapolated to zero power to determine the actual value. Few important systematics will be discussed here that require auxiliary measurements to find out them or can be estimated by combining strengths of the applied electromagnetic fields with high-accuracy calculations of relevant physical properties of the transitions in the clock candidates. Of course, it is important to consider a suitable many-body method for such theoretical calculations. Particularly, at least four reasons can be cited to justify that it is enviable interest to carry

out theoretical studies of the above properties especially for the atomic clocks: (i) as has been demonstrated before, it is feasible to select an atomic system to check its viability for the frequency standard prospectus with accurate knowledge of atomic spectroscopy; (ii) when the experimental results are either not available or carrying out precise measurements is extremely strenuous, theoretical results can be their substitutes; (iii) performing high-precision calculations at the level of present interest can be much economical than setting up their auxiliary experiments; and (iv) comparison between the measurements and calculations of spectroscopic properties in a system obtained from the clock studies could serve as tool to assess the potential of the employed many-body methods.

Quadratic Zeeman Shift

In the presence of static magnetic field, the spectral lines of an atomic system can be split into several components as known from the Zeeman effect. In most of the atomic clocks, linear Zeeman shifts are almost canceled out, while the quadratic Zeeman shifts still contribute to the uncertainties. The interaction operator to determine the quadratic Zeeman shift due to the hyperfine interaction subjected to the external magnetic field $\vec{B} = |B|\hat{z}$ is given by

$$H_B = A_{\text{hf}}\vec{I}\cdot\vec{J} + g_J\mu_B\vec{J}\cdot\vec{B} + g_I\mu_B\vec{I}\cdot\vec{B}, \quad (5)$$

where g_J is the gyromagnetic constant of the electronic state of angular momentum J , g_I is the gyromagnetic constant of the nuclear state with spin I , and μ_B is the Bohr magneton. This shift can be estimated if the hyperfine constants and g -factors for both the electronic and nuclear components of the system known. A_{hf} values can be extracted by measuring hyperfine splitting; however, such procedure is complicated in a fermionic system with $I > 1/2$ when the second- or higher-order hyperfine interactions can be significantly contributing. Due to limited scope, only few examples of comparison between the experimental and theoretical results are provided later. Theoretically, A_{hf} of a state is calculated by

$$A_{\text{hf}} = \frac{\mu_n}{I} \frac{\langle J \| H_{\text{hf}}^{\text{mag}} \| J \rangle}{\sqrt{J(J+1)(2J+1)}}, \quad (6)$$

for the nuclear magnetic moment $\mu_n = \mu_I\mu_B$ where μ_I is the nuclear moment in units of μ_B and $\langle J \| H_{\text{hf}}^{\text{mag}} \| J \rangle$ is the reduced matrix element of the electronic component of the magnetic-dipole hyperfine interaction Hamiltonian $H_{\text{hf}}^{\text{mag}}$.

Similarly, the g_J -factor can be measured precisely or can be evaluated using the expression

$$g_J\langle J \rangle = -\langle JJ | m_e c \sqrt{2} i r \{ \vec{a} \otimes C^{(1)} \}^{(1)} | JJ \rangle \quad (7)$$

with the Dirac matrix \vec{a} and Racah operator C .

Two other approaches are adopted to obtain more precise values of g_J -factors of the bound electrons. The expression given in Eq. (7) is basically for determining the Dirac g_J -factor of a bound electron analogous to $g_D = 2$ for a free electron. However, QED correction yields

$$g_D = 2 \left[1 + \frac{\alpha_e}{2\pi} - 0.328 \frac{\alpha_e^2}{\pi^2} + \dots \right] \approx 2 \times (1.01160). \quad (8)$$

Accounting full QED effects for bound electrons in the atomic systems with more than three electrons is kind of intractable. The QED corrections, however, can be approximated roughly using the interaction Hamiltonian [15]

$$\delta g_J = 0.001160 \beta \Sigma_0^{(1)}, \quad (9)$$

where β and $\Sigma_0^{(1)}$ are the Dirac matrix and the z -component of the Dirac spinor Σ , respectively.

It is also appropriate to estimate only the bound-state relativistic correction to g_J as [16]

$$\Delta g_J = \langle (\beta - 1)2J - \beta L \rangle, \quad (10)$$

for the orbital angular momentum operator L . Then, the final g_J -value can be determined by subtracting the above correction from the g_D -value.

Using a classical vector coupling model, g_J can also be estimated reasonably as

$$g_J = 1 + \frac{J(J+1) - l(l+1) + s(s+1)}{2j(j+1)}, \quad (11)$$

where l and s are the orbital and spin angular momentums, respectively. Similarly, g_I can be extracted from the knowledge of g_J - and g -factor of the hyperfine state (g_F) using the relation

$$g_F = g_J \frac{F(F+1) + J(J+1) - I(I+1)}{2F(F+1)} + g_I \frac{F(F+1) - J(J+1) + I(I+1)}{2F(F+1)} \quad (12)$$

for the I - and J -coupled hyperfine angular momentum F .

Quadratic Stark Shift

The change in the energy of an atomic state $|\Psi_n\rangle$ with angular momentum and its z -component of the state as j_n and m_j placed in an external weak electric field $\vec{E} = |E|\hat{z}$ is given by

$$\Delta E_n(j_n, m_j) \simeq -\frac{1}{2}\alpha_n^{E1} E^2 \quad (13)$$

where α_n^{E1} is the static electric dipole (E1) polarizability of the state. If the electric field is of ac type with altering frequency ω , it yields

$$\alpha_n^{E1} = -\sum_{k \neq n} \langle \Psi_n | D | \Psi_k \rangle^2 \times \left[\frac{1}{(E_n - E_k) + \omega} + \frac{1}{(E_n - E_k) - \omega} \right], \quad (14)$$

where D is the E1 operator and E_i is the energy of the $|\Psi_i\rangle$ state. The sum over k denotes contributions from all possible E1 transitions. Using the tensor product formalism, it becomes

$$\begin{aligned} \alpha_n^{E1} = & \alpha_n^{E1}(0) + A \cos \theta_k \frac{m_j}{j_n} \alpha_n^{E1}(1) \\ & + \left\{ \frac{3 \cos^2 \theta_p - 1}{2} \right\} \left\{ \frac{3m_j^2 - j_n(j_n + 1)}{j_n(2j_n - 1)} \right\} a_n^{E1}(2). \end{aligned} \quad (15)$$

Here A , θ_k , and θ_p are the degree of circular polarization angle, angle between the wave vector of the electric field σ and the \hat{z} -axis, and angle between the direction of polarization and \hat{z} -axis, respectively. Here it should be noted that $A = 0$ for the linearly polarized light and $A = 1(-1)$ for the right(left)-handed circularly polarized light. In the absence of magnetic field, $\cos \theta_k = \cos \theta_p = 1$. In the above expression $\alpha_n^{E1}(0)$, $\alpha_n^{E1}(1)$, and $\alpha_n^{E1}(2)$ are known as scalar, vector, and tensor polarizabilities, respectively, and are usually defined in terms of m_j independent factors (reduced matrix elements) to evaluate them conveniently and given by

$$\begin{aligned} \alpha_n^{E1}(0) = & \frac{(\sum_q 1)(\sum_{m_j} 1)}{3(2j_n + 1)} \sum_{j_k \neq j_n} |\langle J_n \| d \| J_k \rangle|^2 \\ & \times \left[\frac{1}{(E_n - E_k) + \omega} + \frac{1}{(E_n - E_k) - \omega} \right], \end{aligned} \quad (16)$$

$$\begin{aligned} \alpha_n^{E1}(1) = & -\frac{(\sum_q 1)(\sum_{m_j} 1)}{3(2j_n + 1)} \sqrt{\frac{54 j_n(2j_n + 1)}{(j_n + 1)}} \sum_{j_k \neq j_n} (-1)^{j_n + j_k + 1} \begin{Bmatrix} j_n & 1 & j_n \\ 1 & j_k & 1 \end{Bmatrix} \\ & \times |\langle J_n \| d \| J_k \rangle|^2 \times \left[\frac{1}{(E_n - E_k) + \omega} - \frac{1}{(E_n - E_k) - \omega} \right], \end{aligned} \quad (17)$$

and

$$\alpha_n^{E1}(2) = -2 \frac{(\sum_q 1)(\sum_{m_j} 1)}{3(2j_n + 1)} \sqrt{\frac{15 j_n (2j_n + 1)(2j_n - 1)}{2(j_n + 1)(2j_n + 1)}} \\ \sum_{j_k \neq j_n} (-1)^{j_n + j_k + 1} \left\{ \begin{matrix} j_n & 2 & j_n \\ 1 & j_k & 1 \end{matrix} \right\} \\ \times |\langle J_n \| d \| J_k \rangle|^2 \times \left[\frac{1}{(E_n - E_k) + \omega} + \frac{1}{(E_n - E_k) - \omega} \right]. \quad (18)$$

Here q corresponds to the z-component of rank of D . It is obvious that for the static (dc) electric fields, contributions due to the vector polarizability vanishes and also contributions from both $\alpha_n^{E1}(1)$ and $\alpha_n^{E1}(2)$ to the closed-shell configurations nullify.

In the hyperfine $|I j_n F_n m_F\rangle$ state the Stark shift is given, analogously, by

$$\Delta E_n(F_n, m_F) \simeq -\frac{1}{2} \alpha_{n,F}^{E1} E^2, \quad (19)$$

where $\alpha_{n,F}^{E1}$ is the corresponding dipole polarizability and can also be expressed in terms of scalar, vector, and tensor components as before. Since it is hindered to work with the hyperfine states for practicality, the hyperfine state polarizabilities are expressed in terms of the atomic polarizabilities by relating $\alpha_{n,F}^{E1}$ with α_n^{E1} in the IJ-coupling approximation as

$$\alpha_{n,F}^{E1}(0) = \alpha_n^{E1}(0), \quad (20)$$

$$\alpha_{n,F}^{E1}(1) = (-1)^{j_n + I + F} \sqrt{\frac{4 F_n (2F_n + 1)(2j_n + 1)(j_n + 1)}{9(F_n + 1)j_n}} \left\{ \begin{matrix} F_n & J_n & I \\ j_n & F_n & 1 \end{matrix} \right\} \alpha_n^{E1}(1) \quad (21)$$

and

$$\alpha_{n,F}^{E1}(2) = (-1)^{j_n + I + F} \sqrt{\frac{F_n (2F_n - 1)(2F_n + 1)(2j_n + 3)(2j_n + 1)(j_n + 1)}{(2F_n + 3)(F_n + 1)j_n(2j_n - 1)}} \\ \left\{ \begin{matrix} F_n & j_n & I \\ j_n & F_n & 2 \end{matrix} \right\} \alpha_n^{E1}(2). \quad (22)$$

So with accurate knowledge of the atomic polarizabilities and strengths of the applied electric fields, Stark shifts for the frequency standards can be deduced.

Electric-Quadrupole Shift

Electric-quadrupole shifts occur due to interaction between the atomic electric-quadrupole moments with the external electric-field gradients that are generated by

the electrodes of the trapping systems. The Hamiltonian describing the interaction of external electric-field gradient with the atomic quadrupole moment of an atomic state is given by

$$H_Q = \vec{\nabla} E^{(2)} \cdot \vec{\Theta}^{(2)} = \sum_{q=-2}^2 (-1)^q \nabla E_q^{(2)} \Theta_{-q}^{(2)}, \quad (23)$$

where $\vec{\nabla} E^{(2)}$ is the tensor describing the gradient of the external electric field at the position of the atom and $\vec{\Theta}^{(2)}$ is the electric-quadrupole operator. In the principal-axis frame H_Q reads out

$$H_Q = -2 A \Theta_0^{(2)'} + \sqrt{\frac{2}{3}} \epsilon A (\Theta_2^{(2)'} + \Theta_{-2}^{(2)'}). \quad (24)$$

The first-order correction due to H_Q in the hyperfine state $|I j_n F_n m_F\rangle$ is given by

$$\begin{aligned} \Delta E_Q &= \langle I j_n F_n m_F | H_Q | I j_n F_n m_F \rangle \\ &= \frac{-2[3M_F^2 - F(F+1)]A \langle I j_n F_n || \Theta^{(2)} || I j_n F_n \rangle}{[(2F_n + 3)(2F_n + 2)(2F_n + 1)2F_n(2F_n - 1)]^{1/2}} \\ &\quad \times [(3 \cos^2 \beta - 1) - \epsilon \sin^2 \beta (\cos^2 \alpha - \sin^2 \alpha)], \end{aligned} \quad (25)$$

where α , β , and γ are the standard Euler angles that convert the actual principal-axis frame to the working laboratory frame (taking $\gamma = 0$), ϵ is known as asymmetry parameter and A is the strength of the field gradient of the applied direct current (dc) voltage. The reduced matrix element in the above expression is given by

$$\langle I j_n F_n | \Theta^{(2)} | I j_n F_n \rangle = (-1)^{I+j_n+F_n} (2F_n + 1) \begin{Bmatrix} j_n & 2 & j_n \\ F_n & I & F_n \end{Bmatrix} \begin{pmatrix} j_n & 2 & j_n \\ -j_n & 0 & j_n \end{pmatrix}^2 \Theta(j_n). \quad (26)$$

for the atomic quadrupole moment $\Theta(j_n)$. By knowing accurate $\Theta(j_n)$ values of the atomic states involved in a clock transition, differential quadrupole shift of a transition can be obtained. The quadrupole moment of an atomic level with angular momentum j_n is evaluated by

$$\Theta(j_n) = \langle j_n j_n | \Theta_0^{(2)} | j_n j_n \rangle \quad (27)$$

with $\Theta_0^{(2)} = \frac{\epsilon}{2} \Sigma (3z^2 - r^2)$. In an experiment, $\Theta(j_n)$ is measured by altering static dc voltage and is a challenge to extract precisely. Several calculations of this quantity are also available with accuracies as par with the measurements and even in some cases accuracies in the calculations have surpassed over their corresponding measurements.

Multipolar BBR Shifts

Shifts in the quantum energy levels owing to the atom residing in an environment at finite temperature at which an atom can emit radiations with wavelengths depending on the magnitude of temperature are known as BBR shift. Atomic clocks are advised to operate at the room temperature for the general use and the wavelengths emitted from the atoms at this temperature are typically in the infrared region of the electromagnetic spectrum. Accurate estimates of BBR shifts for the laboratory as well as those used in the spacecraft atomic clocks are inevitable as even in the most remote place of intergalactic space, an isolated atom is still subject to cosmic microwave background radiation (CMBR). Uncertainties in the estimated BBR shifts can impose limits to achieve the best atomic clocks. These shifts can be estimated using the multipole expansion of the electromagnetic field. Usually contribution due to the E1 channel is taken into account for its dominant contribution; however, contributions from other higher multipoles, especially from the M1 and E2 channels, can also be significant when the accuracy of clocks reach below 10^{-19} level. A general theory of BBR shift follows below.

The Hamiltonian describing interactions between the electrons in an atomic system with the external propagating electromagnetic field in the Coulomb gauge coupling is given by

$$V(r, \omega) = -c\vec{\alpha} \cdot \vec{A}(r, \omega) = -c(\vec{\alpha} \cdot \vec{\epsilon})e^{i\vec{k} \cdot \vec{r}}, \quad (28)$$

where ω is the angular frequency of the field and $\vec{k} = |k|\hat{k}$ and $\vec{\epsilon}$ are its wave vector and polarization direction, respectively. The expression for the BBR shift of an atomic energy level $|\Psi_n\rangle$ with energy E_n is given by

$$\Delta E_{\text{BBR}} = \frac{1}{2} \sum_{m, \omega} |V_{nm}(r, \omega)|^2 \left(\frac{E_n - E_m}{(E_n - E_m)^2 - \omega^2} \right), \quad (29)$$

for $V_{nm}(r, \omega)$ being the transition matrix of $V(r, \omega)$ between the states $|\Psi_n\rangle$ and $|\Psi_m\rangle$.

Carrying out multipolar expansion of $V(r, \omega)$ in terms of general moments $Q_{LM}^\lambda(\vec{k} \cdot \vec{r})$, it can give

$$\begin{aligned} (\vec{\alpha} \cdot \vec{\epsilon})e^{i\vec{k} \cdot \vec{r}} &= -\sum_{LM} \frac{(K^L)(i^{L+1+\lambda})}{(2L+1)!!} [\vec{Y}_{LM}^\lambda(\hat{k}) \cdot \vec{\epsilon}] \sqrt{\frac{4\pi(2L+1)(L+1)}{L}} Q_{LM}^\lambda(\vec{k} \cdot \vec{r}) \\ &= -\sum_{LM,l} \frac{(K^L)(i^{L+1+\lambda})}{(2L+1)!!} Y_{LM}^\lambda(k_l) \sqrt{\frac{4\pi(2L+1)(L+1)}{L}} Q_{LM}^\lambda(r_l), \end{aligned} \quad (30)$$

where k_l is the component of \vec{k} projecting toward the l th unit vector of $\vec{\epsilon}$, and $\lambda = 1$ and $\lambda = 0$ correspond to the electric and magnetic multipoles, respectively. Since emission from BBR is isotropic, each component of the electric and magnetic fields is related to the spectral energy density as

$$u(\omega, T) = \frac{3}{8\pi} E_I^2(\omega) = \frac{3}{8\pi} B_I^2(\omega) = \frac{1}{\pi^2 c^3} \frac{\omega^3}{e^{\omega/k_B T} - 1}. \quad (31)$$

Hence, averaging over polarizations and propagation directions in Eq. (29), we get [17, 18]

$$\Delta E_{\text{BBR}}^{\lambda, L} = -\frac{\alpha k^B T}{2j_n + 1} \sum_{L, M}^{\neq n} |\langle \Psi_n \| Q_{LM}^\lambda \| \Psi_m \rangle|^2 \times F_L \left(\frac{E_n - E_m}{k_B T} \right), \quad (32)$$

where the universal function is defined as $F_L(y) = \frac{1}{\pi} \frac{L+1}{L(2L+1)!!(2L-1)!!} \times \int_0^\infty dx \left(\frac{1}{y+x} + \frac{1}{y-x} \right) \frac{x^{2L+1}}{e^x - 1}$ that is applicable to all atoms with argument y depending on the range of the atomic parameters. With $|y| \gg 1$, corresponding to the transition energy much larger than the $k_B T$ values as of our interest and for the dominant term $L = 1$, we have

$$\Delta E_{\text{BBR}}^\lambda = -\frac{1}{2c_n^{Q_L^\lambda}} \left(\frac{8\pi^3 \alpha_e^3 (k_B T)^4}{45(2j_n + 1)} \right) \alpha_n^{Q_L^\lambda}(0), \quad (33)$$

where α_e is the fine-structure constant and $\alpha_n^{Q_L^\lambda}(0)$ is the scalar polarizability defined as

$$\alpha_n^{Q_L^\lambda}(0) = C_n^{Q_L^\lambda} \sum_{m \neq n} \frac{|\langle \Psi_n \| Q_{LM}^\lambda \| \Psi_m \rangle|^2}{E_n - E_m}, \quad (34)$$

with the appropriate angular coefficient $C_n^{Q_L^\lambda} = \frac{2}{\alpha_e^{2(\lambda-1)} (2L+1)(2j_n+1)}$ due to the radiative moment Q_L^λ . Usually large contribution comes from E1, followed by M1, then E2, and so on. On average over polarization, the BBR shifts from the first three important channels are given by

$$\Delta E_{\text{BBR}}^{E1} = -\frac{1}{2} \frac{4\pi^3 \alpha_e^3}{15} (k_B T)^4 \alpha_n^{E1}(0) = -\frac{1}{2} \langle E_{E1}^2(\omega) \rangle \alpha_n^{E1}(0), \quad (35)$$

$$\Delta E_{\text{BBR}}^{M1} = -\frac{1}{2} \frac{4\pi^3 \alpha_e^5}{15} (k_B T)^4 \alpha_n^{M1}(0) = -\frac{1}{2} \alpha_e^2 \langle B_{M1}^2(\omega) \rangle \alpha_n^{M1}(0) \quad (36)$$

and

$$\Delta E_{\text{BBR}}^{E2} = -\frac{1}{2} \frac{8(\alpha\pi)^5}{189} (k_B T)^6 \alpha_n^{E2}(0) = -\frac{1}{2} \langle E_{E2}^2(\omega) \rangle \alpha_n^{E2}(0), \quad (37)$$

where $\alpha_n^{M1}(0)$ and $\alpha_n^{E2}(0)$ are the scalar M1 and E2 polarizabilities, respectively, and $\langle E_{E1}^2(\omega) \rangle$, B_{M1}^2 , and $\langle E_{E2}^2(\omega) \rangle$ are the averaged E1-induced electric,

M1- induced magnetic, and E2-induced electric fields, respectively. Conventionally, the above shifts are expressed as functions of temperature scaled with respect to the room temperature ($T = 300^\circ\text{K}$) as

$$\Delta E_{\text{BBR}}^{E1}(300^\circ\text{K}) = -\frac{1}{2} \left(831.9 \frac{V}{m} \right)^2 \left[\frac{T(K)}{300} \right]^4 \alpha_n^{E1}(0), \quad (38)$$

$$\Delta E_{\text{BBR}}^{M1}(300^\circ\text{K}) = -\frac{1}{2} (2.77 \times 10^{-6} \text{Tesla})^2 \left[\frac{T(K)}{300} \right]^4 \alpha_n^{M1}(0), \quad (39)$$

and

$$\Delta E_{\text{BBR}}^{E2}(300^\circ\text{K}) = -\frac{1}{2} \left(7.2 \times 10^{-3} \frac{V}{m} \right)^2 \left[\frac{T(K)}{300} \right]^6 \alpha_n^{E2}(0). \quad (40)$$

Even for estimating the E1 BBR shift, the above formula does not take into account frequency distribution properly. Including the appropriate dynamic correction, the final expression for the BBR shift due to the E1 component yields

$$\Delta E_{\text{BBR}}^{E1}(300^\circ\text{K}) = -\frac{1}{2} \left(831.9 \frac{V}{m} \right)^2 \left[\frac{T(K)}{300} \right]^4 \alpha_n^{E1}(0) [1 + \eta(\alpha_n^{E1}, T)], \quad (41)$$

where

$$\eta(\alpha_n^{E1}, T) = \frac{\left(\frac{80}{63}\right) \pi^2}{\alpha_n^{E1}(0) T} \sum_{m \neq n} \frac{|\langle j_n \| D \| j_m \rangle|^2 T^3}{(2j_n + 1)(E_n - E_m)^3} \left(1 + \frac{21\pi^2 T^2}{5(E_n - E_m)^2} + \frac{336\pi^4 T^4}{11(E_n - E_m)^4} \right).$$

Relativistic Many-Body Methods

As mentioned at several occasions, it is possible to estimate many important systematics for the atomic clocks and propose new clock candidates by the theoretical studies. This warrants for development of suitable many-body methods that are capable of considering the electron correlation effects more effectively. It is also evident from most of the undertaken examples that consideration of a suitable atomic transition with one of the atomic states having almost-degenerate fine-structure partner has many merits, e.g., achieving high stability and accuracy, for the optical frequency standards. This urges for using relativistic mechanics in the theoretical studies. Moreover, almost all the candidates considered for frequency standards are relatively heavy atomic systems for which accurate calculations of their properties necessitates employing valid relativistic many-body methods. Consideration of a fully relativistic theory in its covariant form is impractical in the many-electron bound systems. Working with Dirac Hamiltonian for electrons along with nuclear potential and Coulomb repulsion between the electrons can suffice the present goal

to accomplish calculations within the required accuracy. Nevertheless, corrections from higher relativistic effects at the leading orders, e.g., Breit interaction due to exchange of transverse photons and quantum electrodynamics (QED), can be incorporated to augment the calculated results.

General Approach

The Dirac–Coulomb (DC) Hamiltonian for an atomic system is given by

$$H_{\text{DC}} = \sum_i [c \vec{\alpha}_i \cdot \vec{p}_i + \beta_i c^2 + V_n(r_i)] + \sum_{i \geq j} \frac{1}{r_{ij}} \quad (42)$$

(in atomic unit (au)), where $\vec{\alpha}$ and β are the Dirac matrices and $V_n(r)$ is the nuclear potential. This is a good approximation to describe the positive energy states of the Dirac theory. Weak coupling with the positron wave functions are usually neglected and also the rest mass energy of the electrons can be subtracted for the convenience. Thus, the working DC Hamiltonian reads out

$$H_{\text{DC}} = \sum_i [c \vec{\alpha}_i \cdot \vec{p}_i + (\beta_i - 1) c^2 + V_n(r_i)] + \sum_{i \geq j} \frac{1}{r_{ij}}. \quad (43)$$

Again, it may not be appropriate to assume atomic nucleus as a point- like object for accurate calculations. On the other hand, there are not proper valid models available to describe the nuclear structure exactly. Among many, Fermi charge distribution model is more popular in which density of an electron within the atomic nucleus is described by

$$\rho_n(r) = \frac{\rho_0}{1 + e^{(r-b)/a}}, \quad (44)$$

where ρ_0 is the normalization factor, b is known as half-charge radius and $a = 2.3/(4 \ln 3)$ is related to the skin thickness of the nucleus. Considering this distribution, the nuclear potential can be obtained as

$$V_n(r) = \frac{Z}{\aleph r} \begin{cases} \frac{1}{b} \left(\frac{3}{2} + \frac{a^2 \pi^2}{2b^2} - \frac{r^2}{2b^2} + \frac{3a^2}{b^2} P_2 + \frac{6a^3}{b^2 r} (S_3 - P_3^+) \right) & \text{for } a \geq b \\ \frac{1}{r} \left(1 + \frac{a^2 \pi^2}{b^2} - \frac{3a^2 r}{b^3} P_2^- + \frac{6a^3}{63b} (S_3 - P_3^-) \right) & \text{for } r \geq b, \end{cases} \quad (45)$$

for the factors $\aleph = 1 + \frac{a^2 \pi^2}{b^2} + \frac{6a^3}{b^3} S_3$ with $S_k = \sum_{m=1}^{\infty} \frac{(-1)^{m-1}}{m^k} e^{-b/a}$ and $P_k^{\pm} = \sum_{m=1}^{\infty} \frac{(-1)^{m-1}}{m^k} e^{\pm m(r-b)/a}$. The b -parameter can be determined from $b = \sqrt{\frac{5}{3} r_{\text{rms}}^2 - \frac{7}{3} a^2 \pi^2}$ with the root mean square radius r_{rms} , which can be estimated using the empirical formula $r_{\text{rms}} = 0.836A^{1/3} + 0.57$ in fermi (fm) or can be taken from a standard nuclear data table.

We now turn to outline procedures to estimate corrections due to higher-order relativistic effects. Since the nuclear potential is the dominating contributing term in the above DC Hamiltonian, the QED effects are estimated by treating the nuclear potential as the strong external electromagnetic field seen by the bound electrons in an atomic system. Thus, an effective potential is defined accounting lower-order vacuum polarization (VP) and self-energy (SE) QED effects [19] in place of $V_n(r)$ in the atomic Hamiltonian and reads

$$V_{\text{eff}}(r) = [1 + V_U(r) + V_{\text{WC}}(r) + V_{\text{mg}}(r) + V_{\text{el}}(r)]V_n(r), \quad (46)$$

where $V_U(r) = \frac{2\alpha_e}{3\pi} \int_1^\infty dt \frac{\sqrt{t^2-1}}{t^2} (1 + \frac{1}{2t^2}) e^{-2ctr}$ and $V_{\text{WC}}(r) = -\frac{4\alpha_e}{9\pi} \frac{0.092 Z^2 \alpha_e^2}{1+(1.62cr)^4}$ are the Uehling and Wichmann–Kroll corrections, respectively, representing the lower-order VP effect and the SE effect is taken through the magnetic form-factor $V_{\text{mg}}(r) = \frac{\alpha_e}{4\pi c} i\gamma \cdot \Delta \left[V_n(r) \left(\int_1^\infty dt \frac{1}{t\sqrt{t^2-1}} e^{-2ctr} - 1 \right) \right]$ and the electric form-factor $V_{\text{el}}(r) = -\frac{\alpha_e}{\pi} \int_1^\infty dt \frac{1}{t\sqrt{t^2-1}} \left[\left(1 - \frac{1}{2t^2}\right) \left[\ln(t^2 - 1) + \ln\left(\frac{4c^2}{\lambda^2}\right) \right] - \frac{3}{2} + \frac{1}{t^2} \right] e^{-2ctr}$ for the cutoff parameter chosen cautiously as $\lambda \sim (Z\alpha_e^2)c$.

The potential due to the Breit interaction between the electrons located at the i th and j th positions is given by

$$V_B(r_{ij}) = -\frac{1}{2r_{ij}} \{ \alpha_i \cdot \alpha_j + (\alpha_i \cdot \hat{r}_{ij})(\alpha_j \cdot \hat{r}_{ij}) \}. \quad (47)$$

Owing to the two-body nature of the Coulomb and Breit interactions, solving eigenvalue equation for the atomic Hamiltonian H_{at} (with only Coulomb or both Coulomb and Breit interactions), given by

$$H_{\text{at}} | \Psi_n^{(0)} \rangle = E_n | \Psi_n^{(0)} \rangle, \quad (48)$$

with more than three electrons in an atomic system is infeasible. Instead, it is a usual practice to get the approximated solution to the above equation and then append corrections from the residual contributions gradually. This approximated solution is treated as a model space in the working Hilbert or Fock space accounting majority of the contributions from the Coulomb (and Breit) interaction(s) in the calculation of the atomic wave functions. One of the most conducive and appropriate approaches to determine the approximated wave functions is to use the Hartree–Fock (Dirac–Fock (DF) in the relativistic framework) Hamiltonian (H_0). The residual interaction ($V_{\text{res}} = H_{\text{at}} - H_0$) can further improve the results by annexing contributions from the rest of the Hilbert or Fock space, referred to as orthogonal space, through a decent many-body method. Below we demonstrate few methods and try to inculcate one-to-one connections among these methods. For this purpose, we try to build up each many-body approach by commencing from the same DF wave function. To proceed further, we adopt the procedure of the generalized Bloch equation to explain the many-body methods systematically in a comprehensible and logical manner. In the

many-body perturbation theory (MBPT), the exact wave function of an atomic state can be expressed as

$$|\Psi_n^{(0)}\rangle = \Omega_n^{(0)}|\Phi_n\rangle, \quad (49)$$

where $|\Phi_n\rangle$ is the model space (here DF wave function) and $\Omega_n^{(0)}$ is the wave operator which is responsible for incorporating contributions from the orthogonal space due to V_{res} . Orthogonal space contributions can either be expressed in terms of the order of perturbation or in the form of excited configurations with respect to $|\Phi_n\rangle$. For the simple reason, we can go on with the perturbation series expansion approach first and then we can manifest the same in terms of the excited state configurations.

Two projection operators P and Q satisfying $|\Phi_n\rangle = P|\Psi_n^{(0)}\rangle$ and $Q = I - P$ for the identity operator I are defined for easy description, which follows $P = |\Phi_n\rangle\langle\Phi_n|$. In the perturbative approach, it yields

$$\Omega_n^{(0)} = \Omega_n^{(0,0)} + \Omega_n^{(1,0)} + \Omega_n^{(2,0)} + \dots = \Sigma_k \Omega_n^{(k,0)}. \quad (50)$$

Notice that we use two superscripts, for the later use, among which the first one represents the number of V_{res} present in the calculations, while the second one with zero means there is no external source of perturbation taken into account. The amplitudes of the above wave operators are solved one by one in the sequence of order of perturbations involved with the wave operators using the following recursive relation:

$$[\Omega_n^{(k,0)}, H_0]P = QV_{\text{res}}\Omega_n^{(k-1,0)}P - \Sigma_{m=1}^{k-1}\Omega_n^{(k-m,0)}P V_{\text{res}}\Omega_n^{(m-1,0)}P. \quad (51)$$

The energy of the state (E_n) can be evaluated using an effective Hamiltonian $H_n^{\text{eff}} = PH\Omega_n^{(0)}P$ at different orders of perturbation with the expansion form of $\Omega_n^{(0)}$. That is, $E_n = \langle\Phi_n|H_n^{\text{eff}}|\Phi_n\rangle$.

There are, specifically, two approaches adopted to evaluate dipole polarizability of an atomic state. In a conventional approach, the energy of the $|\Psi_n\rangle$ state of an atom placed in an isotropic electric field of strength ε changes as [20, 21]

$$E_n(\varepsilon) = E_n(0) - \frac{\alpha_n^{E_1}}{2}\varepsilon^2 - \dots, \quad (52)$$

where $E_n(0)$ and $E_n(\varepsilon)$ are the total energies of the state in the absence and presence of the electric field, respectively. This approach requires mixed parity orbitals to calculate the atomic energy in the presence of the electric field, which are practically cumbersome using the spherical coordinate systems but are manifested using the molecular methods (in the Cartesian coordinate system).

Alternatively, the modified wave function ($|\Psi_n\rangle$) of the atomic system in the presence of an external weak perturbative source (V_{prt}) can be approximated to first-order approximation as

$$|\Psi_n\rangle = |\Psi_n^{(0)}\rangle + \lambda |\Psi_n^{(1)}\rangle, \quad (53)$$

where λ is an arbitrary parameter (corresponds to ε in the evaluation of α_n^{E1}) representing the strength of the perturbation source. In this way, α_n^{E1} can be obtained by expressing [22–26]

$$\alpha_n^{E1} = \frac{\langle \Psi_n | D | \Psi_n \rangle}{\Psi_n | \Psi_n} \simeq \frac{\langle \Psi_n^{(0)} | D | \Psi_n^{(1)} \rangle}{\Psi_n^{(0)} | \Psi_n^{(0)}}, \quad (54)$$

by considering $V_{\text{prt}} \equiv \varepsilon D \hat{z}$ for small values of ε .

It is commanding to obtain solution for $|\Psi_n^{(1)}\rangle$ by solving an inhomogeneous equation of the type

$$[(H_n^{\text{eff}} - E_n) | \Psi_n^{(1)} \rangle = (E_n^1 - V_{\text{prt}}) | \Psi_n^{(0)} \rangle, \quad (55)$$

analogous to the approach proposed and implemented by Dalgarno [27]. In Bloch equation methodology, we can express $|\Psi_n^{(1)}\rangle = \Omega_n^{(1)} |\Phi_n\rangle$ such as $\Omega_n^{(1)} = \sum_k \Omega_n^{(k,1)}$ encompassing k th order of V_{res} and one order external perturbation V_{prt} . The amplitudes of $\Omega_n^{(1)}$ are obtained from the following equation [26]:

$$[\Omega_n^{(k,1)}, H_0] P = Q [V_{\text{prt}} \Omega_n^{(k,0)} + V_{\text{res}} \Omega_n^{(k-1,1)}] P - \sum_{m=1}^{k-1} (\Omega_n^{(k-m,0)} P V_{\text{prt}} \Omega_n^{(m,0)} P - \Omega_n^{(k-m,1)} P V_{\text{res}} \Omega_n^{(m,0)} P). \quad (56)$$

For the choice of reference state $|\Phi_n\rangle$ as the DF wave function and external perturbation operator V_{prt} being a one-body operator, the zeroth-order expressions for the wave operators can yield $\Omega_n^{(0,0)} = 1$, $\Omega_n^{(1,0)} = 0$, and $\Omega_n^{(0,1)} = \sum_{p,a} \frac{\langle p | V_{\text{prt}} | a \rangle}{\epsilon_p - \epsilon_a}$ for the occupied a and unoccupied p -orbitals with energies ϵ_a and ϵ_p , respectively. In the double perturbative sources, up to $k = 0, 1, 2 \dots$ approximations in the wave operators are referred to MBPT(1) or DF, MBPT(2), MBPT(3), etc. methods, respectively.

Having said and done with the basic formalism of determining atomic wave functions in the many-body perturbative analysis, extending them to build up these wave functions containing all orders in V_{res} for both the cases, the absence and presence of external source, would be now much straightforward. This can be achieved by generalizing the above perturbative approaches after carefully formulating the wave operator Ω_n in a slight different form or assembling the coefficients from each order of perturbation expansion to compose various degrees of excitations. We discuss few important all-order many-body methods that are widely used in the studies of atomic clock pertinent physics; specifically, two all-order perturbative approaches known as **configuration interaction (CI)** and

coupled-cluster (CC) methods in the absence of external field and their extensions to deal with weak external interaction up to the first-order perturbation.

Configuration Interaction (CI) Method

As mentioned above, the exact wave function $|\Psi_n^{(0)}\rangle$ can be expressed in terms of excited configurations with respect to $|\Phi_n\rangle$. Mathematically, this corresponds to

$$\begin{aligned} |\Psi_n^{(0)}\rangle &= |\Phi_n\rangle + \sum_I^{N_I} C_n^I |\Phi_n^I\rangle + \sum_{II}^{N_{II}} C_n^{II} |\Phi_n^{II}\rangle + \sum_{III}^{N_{III}} C_n^{III} |\Phi_n^{III}\rangle + \dots \\ &\equiv \tilde{C}_n \left| \psi_n^{(0)} \right\rangle + \sum_I^{N_I} \tilde{C}_I \left| \psi_I^{(0)} \right\rangle + \sum_{II}^{N_{II}} \tilde{C}_{II} \left| \psi_{II}^{(0)} \right\rangle + \sum_{III}^{N_{III}} \tilde{C}_{III} \left| \psi_{III}^{(0)} \right\rangle + \dots \end{aligned} \quad (57)$$

where $|\Phi_n^K\rangle$ s are the determinants corresponding to DF wave functions for N_K number of possible k th excited states constructed from $|\Phi_n\rangle$ and C_n^* s are their corresponding mixing coefficients. Obviously it is only possible to generate N -tuple excitations for full expansion in a system having N -number of electrons. The above expansion is a direct consequence of the fact that each order in the correction from the perturbed wave functions can be expressed as linear combination of excited states. This also directly follows; the excited state determinants are nothing but the leading part of the excited atomic states. As a result, the calculated atomic state function (ASF) $|\Psi_n^{(0)}\rangle$ can be expressed as a linear combination of configuration state functions (CSFs) representing the trial atomic state functions (denoted by the notation $|\psi_n^{(0)}\rangle$). This approach of constructing atomic wave functions is known as CI method. In a special condition the above excited Slater determinants ($|\Phi_n^*\rangle$) can also be chosen as CSFs in a CI method. By diagonalizing the atomic Hamiltonian with respect to the CSFs, one can obtain the values of the C_k^* or \tilde{C}_k^* coefficients. Although conceptually CI method looks simpler, computationally it is much difficult to account the higher-level excitations and often it has been truncated to only single and double excitations (referred to as CISD method) in the practical applications. It can be shown by considering only the double configurations that the corrections from V_{res} to the wave function calculations in a truncated CI method are proportional to $1/\sqrt{N}$ [20, 28]. This simply means for $N \rightarrow \infty$, the correlation contributions to the calculation diminish (famously known as size-consistency problem). Hence, truncated CI method may not be judicious to employ for accurate calculations of atomic properties in the heavy systems (large N) conceptually and results from the truncated CI can be questionable for their validation. Nevertheless, results close to the experimental values can be achieved by taking only important CSFs from the energy-level configurations in a truncated CI method. Indeed upon the consideration of more Slater determinants in the construction of $|\psi_n^{(0)}\rangle$, it is possible to improve the quality of truncated CI results, and this approach is recognized as multi-configurational Dirac–Fock (MCDF) method.

In a similar approach, the first-order correction to the wave function due to the external field and matrix elements of an operator among different states can be

obtained by mixing CSFs with appropriate parities and angular momentum as per the selection rules.

Coupled-Cluster (CC) Method

In the CC method, linear combination of the Slater determinants are carried out in a distinct manner so that atomic wave functions are contrived to form an exponential function. Starting with the same basic principle as in the CI method, we can rewrite

$$\begin{aligned}
 |\Psi_n^{(0)}\rangle &= |\Phi_n\rangle + \sum_I^{N_I} C_n^I |\Phi_n^I\rangle + \sum_{II}^{N_{II}} C_n^{II} |\Phi_n^{II}\rangle + \sum_{III}^{N_{III}} C_n^{III} |\Phi_n^{III}\rangle + \dots \\
 &\equiv |\Phi_n\rangle + \sum_I^{N_I} T_I^{(0)} |\Phi_n\rangle + \sum_{II}^{N_{II}} T_{II}^{(0)} |\Phi_n\rangle + \sum_{III}^{N_{III}} T_{III}^{(0)} |\Phi_n\rangle + \dots \\
 &= |\Phi_n\rangle + T_1^{(0)} |\Phi_n\rangle + T_2^{(0)} |\Phi_n\rangle + T_3^{(0)} |\Phi_n\rangle + \dots \\
 &= e^{T_1^{(0)} + T_2^{(0)} + T_3^{(0)} + \dots + T_N^{(0)}} |\Phi_n\rangle = e^{T^{(0)}} |\Phi_n\rangle,
 \end{aligned} \tag{58}$$

where $T_k^{(0)} = \sum_K^{N_K} T_K^{(0)}$ for $k = 1, 2, 3 \dots$ represents the CC excitation operator with subscript k implying the k th level excitation carried out from $|\Phi_n\rangle$. The advantage of this method is of manifold: (i) it is both conceptually and computationally simpler, (ii) truncated CC methods also satisfy both size-extensivity and size-consistency properties, (iii) owing to exponential form of the expression for the wave function, contributions from higher-level excitations to a certain extent also do appear through the nonlinear terms in a truncated CC method, etc.

Although we mentioned above about computational simplicity in the use of CC method, in actual practice it may not turn out to be factual. Because of the presence of the nonlinear terms and requirement of a sufficiently large Hilbert or Fock space to carry out accurate calculations of the atomic wave functions, intermediate computational strategy may be required conforming available computational resources and depending upon the size of the atomic system of our interest [20, 22, 26]. This can be judiciously accomplished by devising a proper plan before implementing the method. For example, a well-suited symmetry group and Kramers relations [29] can be adopted to reduce the computational cost when molecular orbitals are used. Since atomic orbitals are meticulously described in the spherical coordinate system, the use of reduced matrix elements instead of actual matrix elements would be more pertinent and can prevail extra computations for the azimuthal quantum numbers. This can be the most well-versed approach for states having closed-shell configurations, but states of open-shell configurations cannot be dealt with this way. However, atomic states having one or two electrons in the valence orbitals and one or two electron less from closed-shell configurations can be computed using the reduced matrix elements by appending valence orbitals or removing electrons from the appropriate closed-shell configurations in the Fock-space approach. We discuss here a few such approaches but restricting to only one electron attachment or removal from the closed-shell configurations.

In the Fock-space CC formalism, wave functions of one valence ($\nu = n$) atomic states are expressed as

$$|\Psi_n\rangle = e^{T_0^{(0)}} \{1 + S_v^{(0)}\} |\Phi_v\rangle, \quad (59)$$

where S_v is a CC operator exciting the valence electron v along with the closed-core $|\Phi_v\rangle$. In a Fock-space approach, $|\Phi_v\rangle$ is constructed from the closed-core $|\Phi_0\rangle$ by appending the respective valence orbital v as $|\Phi_v\rangle = a_v^+ |\Phi_0\rangle$. Likewise, wave functions for the states having less than one electron from the closed-shell configurations can be expressed as

$$|\Psi_a\rangle = e^{T_0^{(0)}} \{1 + R_a^{(0)}\} |\Phi_a\rangle, \quad (60)$$

where R_a is the CC operator responsible for annihilating a core electron ($a = n$) from the closed-core $|\Phi_n\rangle$ and exciting an electron from a reference state $|\Phi_a\rangle$ constructed as $|\Phi_a\rangle = a_a |\Phi_0\rangle$. In both of the above approaches, CC $T_0^{(0)}$ operator is responsible for accounting electron excitations from the closed-core $|\Phi_0\rangle$. In these expressions, superscript (0) is used to highlight that wave functions are still free from the external fields. It is called as CCSD method when only the single and double excitations are taken in, while it is known as CCSDT, CCSDTQ, etc. methods with the inclusion of triples, quadrupoles, and so on excitations, respectively [20]. Since computational complexity increases with the addition of higher-level excitations, CCSD approximation is the prevalent method in the atomic and molecular spectroscopy studies. Contributions from important triples can be included perturbatively through the CCSD method in the CCSD[T], CCSD(T), CCSDpT, and CCSDvT framework [20,25,30] in the same amount of computational requirements to uplift the results further. The matrix element of an operator O between the $|\Psi_f\rangle$ and $|\Psi_i\rangle$ states (for the expectation value $|\Psi_f\rangle = |\Psi_i\rangle$) can be determined by

$$\begin{aligned} \langle O \rangle_{fi} &= \frac{\langle \Psi_f | O | \Psi_i \rangle}{\sqrt{\langle \Psi_f | \Psi_f \rangle \langle \Psi_i | \Psi_i \rangle}} \\ &= \frac{\langle \Phi_f | \{1 + \Omega_f^+\} \sigma \{1 + \Omega_i\} | \Phi_i \rangle}{\sqrt{\langle \Phi_f | \{1 + \Omega_f^+\} \bar{N} \{1 + \Omega_i\} | \Phi_f \rangle \langle \Phi_i | \{1 + \Omega_i^+\} \bar{N} \{1 + \Omega_i\} | \Phi_i \rangle}}, \end{aligned} \quad (61)$$

where Ω_n is either S_n or R_n for the attachment or detachment of an electron case, respectively, and $\bar{O} = e^{T_0^{(0)+}} O e^{T_0^{(0)}}$ and $\bar{N} = e^{T_0^{(0)+}} e^{T_0^{(0)}}$ are two non-truncated series in the above expression. For the closed-shell atomic states ($|\Psi_i\rangle = |\Psi_f\rangle = |\Psi_0\rangle$), it yields [20]

$$\langle O \rangle = \frac{\langle \Psi_0 | O | \Psi_0 \rangle}{\sqrt{\langle \Psi_0 | \Psi_0 \rangle}} = \langle \Phi_0 | \bar{O} | \Phi_0 \rangle_c \quad (62)$$

where the subscript c in the expression represents to only the connected terms. In many cases, only linear terms even in the CCSD method are considered (referred here as LCCSD method) for carrying out the calculations. The above non-truncated series can be computed at several steps [22–26], but it is advisable to use other CC methods like normal CC method with biorthogonal condition, extended CC method, etc. to fend off these non-truncated series [20].

Creating excited states from an atomic state of closed-shell configuration $|\Psi_0\rangle$ in a Fock-space approach is onerous, but an equation-of-motion CC (EOMCC) method is apropos to determine L th level excited states $|\Psi_L(J, \pi)\rangle$ with total angular momentum J and parity π from $|\Psi_0\rangle$. In this approach, it follows [20, 31]

$$|\Psi_L(J, \pi)\rangle = \Omega_L(J, \pi)|\Psi_0\rangle = \Omega_L(J, \pi)e^{T_0^{(0)}}|\Phi_0\rangle = e^{T_0^{(0)}}\Omega_L(J, \pi)|\Phi_0\rangle. \quad (63)$$

By construction both the $T^{(0)}$ and Ω_L operators are similar in nature; hence, they can commute each other, but they commission operationally different roles.

In the presence of an external source, the first-order corrected wave function in the CC method can be expressed as [22–26]

$$|\Psi_n^{(1)}\rangle = e^{T^{(0)}}(T^{(1)})|\Phi_n\rangle \quad (64)$$

Similar to $T^{(0)}$ the perturbed CC operator $T^{(1)}$ excites electrons from $|\Phi_n\rangle$, but parity of $T^{(0)}$ is always even as it originates from the Coulomb (or Breit) operator, while the parity of $T^{(1)}$ can depend on the characteristic of V_{prt} .

Random-Phase Approximation (RPA)

Though **random-phase approximation** is a subclass of CC method, technically it is derived from the DF method in a completely different approach. Its main advantage is that it can embody the core-polarization effects to all orders at the same time being cost effective. Its expression can be obtained from Eq. (56) by continuing k to infinite order for $\Omega^{(k,1)}$ while suppressing $\Omega^{(k,0)}$ in a self-consistent procedure. The derivation of the final expression is a repercussion of expanding the DF wave function $|\Phi_n\rangle$ to first order due to V_{prt} and generalizing it to infinite order. Thence, it only picks up the singly excited configurations from $|\Psi_n\rangle$ in case of polarizability calculations owing to one-body form of the interaction operator $V_{\text{prt}} \equiv D$. In the RPA approach, the first-order corrected wave operator $\Omega_n^{(1)} \equiv \Omega_n^{(\text{RPA})}$ is explicitly given by

$$\Omega_n^{(\text{RPA})} = \sum_{k=1}^{\infty} \sum_{pq,ab} \left\{ \frac{[\langle pb|V_{\text{res}}|aq\rangle - \langle pb|V_{\text{res}}|qa\rangle]\Omega_{b\rightarrow q}^{(k-1,1)}}{\epsilon_p - \epsilon_a} + \frac{\Omega_{b\rightarrow q}^{(k-1,1)+} [\langle pq|V_{\text{res}}|ab\rangle - \langle pq|V_{\text{res}}|ba\rangle]}{\epsilon_p - \epsilon_a} \right\}, \quad (65)$$

where $a \rightarrow p$ implies singly excitation operation by the wave operator replacing an orbital a by p in $|\Phi_n\rangle$.

Demonstration of Few Theoretical Results

The main aim here is to testify the role of relativistic many-body methods for accurate calculations of the quantities that can be useful in various possible ways for the atomic clock studies, especially in the precise estimate of systematics. Proclaiming through only few examples, accurate calculations of A_{hf} constants, g_J -factors, static polarizabilities, and quadrupole moments of atomic states in a number of clock candidates will be demonstrated at different levels of approximations in the employed many-body methods.

A_{hf} -Constants and g_J -Factors

Almost all heavy singly charged ions from the alkaline earth metal group in the periodic table (from Ca to Ra) are either considered or proposed for the atomic clocks because these ions have typically an S-state as the ground state and two excited metastable D-states. In Table 2, a summary of the calculated results for $A_{\text{hf}}/(\mu_I/I)$ of the above states in the alkaline earth ions, Yb^+ and Hg^+ , considering the DF, RCC, and MCDF methods is reported from [6, 8, 32–34]. It has been shown explicitly in these references that accurate calculations of these quantities in the ground and $D_{3/2}$ states require both pair-correlation and core-polarization effects to be considered to all orders, while the core-polarization effects are solely important for the correct evaluation of A_{hf} values in the $D_{5/2}$ states [33]. In fact, these values for the metastable $6D_{3/2}$ state in Ra^+ was first predicted by theory using the CC method and later it was verified by the experiment [35].

Among others, $^{171}\text{Yb}^+$ ion is the most valuable ion for the atomic clock perspectives as its three transitions, the largest among all the elements, are considered for the frequency standards as it has three metastable states ($5d$ -fine-structure levels with lifetimes of the order of few seconds and the first excited $4f^{13} \ ^2F_{7/2}$ state with a lifetime about 6 years). The octopole transition $6s \rightarrow 4f_{7/2}$ of this ion has the uttermost narrow linewidth which is advantageous for making prospective primary frequency standard. Except the $4f_{7/2}$ state, the other three states (including the ground state) of $^{171}\text{Yb}^+$ have three valence orbitals, but they can be treated

Table 2 Comparison between the calculated A_{hf} values divided by I/μ_I from the DF, CC, and MCDF methods against their available experimental results in the alkaline earth ions, Yb^+ and Hg^+ . The MCDF results are mostly taken from [32], while other results are compiled from the electron attachment method of [6, 8, 33, 34] and from the references therein. Here n represents the principal quantum number of the ground state of the corresponding ion

Method	Ca^+	Sr^+	Ba^+	Ra^+	Yb^+	Hg^+
<i>ns</i> state						
DF	1,561.62	3,039.53	4,741.67	14,913.89	9,637.42	34,380.31
CC	2,142.01	4,123.06	6,517.57	19,689.37	13,166.69	41,592.88
MCDF						
Experiment	2,142.02	4,120.04	6,429.83	18,772	12,807.14	40,035.74
$(n-1)d_{3/2}$ state						
DF	88.74	128.30	205.38	293.53	286.67	
CC	125.64	187.64	305.47	441.67	406.14	
MCDF	125.56		308.83		405.55	
Experiment	125.64		303.77	430.67	435.51	
$(n-1)d_{5/2}$ state						
DF	9.18	53.56	+82.58	107.60	109.47	
CC	9.56	-8.83	-19.19	-138.36	-69.88	
MCDF	12.86		+15.03		-12.75	
Experiment	10.34	8.95	-19.25		-64.42	

Table 3 Comparison between the calculated A_{hf} values divided by I/μ_I from the MCDF [32] method and electron detachment theory with DF and CC methods [36] against their available experimental values

	Yb^+		Hg^+	
	$[4f^{14}]6s$ state	$4f^{13}6s^2\ ^2F_{7/2}$ state	$[5d^{10}]6s$ state	$5d^96s^2\ ^2D_{5/2}$ state
DF	7,318.10	878.78	30,050.78	902.43
CC	12,871.96	1,016.87	41,608.82	1,080.29
MCDF				952.29
Experiment	12,807.14	916.60		

as states with one valence configurations with the closed-core $[4f^{14}]$. Also, both the ground and $4f_{7/2}$ states of Yb^+ can be regarded as one electron less than the closed-core $[4f^{14}]6s^2$. Analogously both the states of the clock transition $[5d^{10}]6s^2\ ^2S_{1/2} \rightarrow 5d^96s^2\ ^2D_{5/2}$ in Hg^+ can be calculated in the similar approach. Comparison between the A_{hf} values obtained using different many-body methods and with the available experimental results can be found from Tables 2 and 3. It can be seen from these tables that when A_{hf} of the ground state of Yb^+ is calculated using an electron detachment than attachment approach, the result becomes closer with the experimental value. This is because in the former case the core orbitals see effect due to the valence electron and in the latter approach they come only through the CC operators [36]. It is indeed a quite remarkable observation, though not much difference found in the calculations for Hg^+ (Nandy DK, Private communication).

Table 4 Preparatory calculations of g_J -factors and their δg_J corrections (given within the parentheses) in the states of interest for the clock transitions in Ca^+ from DF and different CC methods and comparison with the semiclassical and available experimental results

Method	$4s^2S_{1/2}$ state	$3d^2D_{3/2}$ state	$3d^2D_{5/2}$ state
DF	1.99995307831	0.799922324299	1.19991738748
	(+0.00284130797)	(−0.000898052128)	(+0.00112057581)
LCCSD	1.99347972816	0.796582101999	1.19726585871
	(+0.00282940412)	(−0.000898459207)	(+0.00111787848)
CCSD	1.99783376440	0.802135504861	1.20140651205
	(+0.00283303463)	(−0.000893389416)	(+0.00111891602)
CCSD(T)	1.99941009011	0.802210930664	1.20151553526
	(+0.00283303788)	(−0.000893393408)	(+0.00111892083)
CCSDvT	1.99942182027	0.802214948013	1.20151548994
	(+0.00283304004)	(−0.000893394022)	(+0.00111893179)
Δ Breit	−0.00000546639	+0.00004031931	+0.00000746347
	(−0.00000000443)	(−0.00000000687)	(+0.00000000212)
Δ QED	−0.00000006897	+0.00000000808	+0.00000000002
	(−0.00000000014)	(+0.00000000004)	(+0.00000000001)
Final	2.00224932	0.801361875	1.20264189
Semiclassical	2.0	0.8	1.2
Experiment [37]	2.00225664(9)		

Lindroth and Ynnerman had critically evaluated Δg_J values of the ground states of Li , Be^+ , and Ba^+ to quite a high accuracy using the CC method in comparison with the experimental values [16]. In Table 4, preliminary calculations of g_J and δg_J values have been demonstrated of the ground and metastable states of Ca^+ using the CC method at different levels of approximations and considering the higher-order relativistic corrections, while the semiclassical formula gives these values as 2, 0.8, and 1.2 for the respective states. In the above table, the ground state value is also compared with its experimental result [37] up to the 4th decimal places. It, thus, clearly advocates in favor of the potential of the CC method to produce results accurately.

Static Polarizabilities (In Au)

Two elegant methods have already been described to evaluate α_n^{E1} values in the atomic systems. To demonstrate the first kind, these values for the $3s^2\ ^1S_0$ and $3s3p\ ^3P_0$ states in Al^+ along with excitation energy between these two states are given in Table 5 by taking two arbitrary values of the electric field as $\varepsilon = 0.001$ au and $\varepsilon = 0.002$ au in an EOMCC method with various levels of approximations [21]. These values are also compared with another latest calculation using the CI+MBPT method in a sum-over-states approach [38].

Table 5 An example of amelioration of α_n^{E1} values for the states of clock transition in Al^+ by estimating second-order energy difference with arbitrary electric fields in the finite gradient method using an EOMCC approach [21]. The final results are also compared with a sum-over-states approach in the CI+MBPT method framework [38]

Method	Excitation energy	$3s^2\ ^1S_0$	$3s3p^3\ P_0$	Differential
CCSD	$37,186 \pm 52$	24.251 ± 0.044	24.656 ± 0.088	0.406 ± 0.042
+Triples	146 ± 33	-0.126 ± 0.011	-0.061 ± 0.015	0.065 ± 0.026
+Quadrupoles	2 ± 4	-0.002 ± 0.005	-0.001 ± 0.002	0.003 ± 0.007
+Breit	-6 ± 6	0.015 ± 0.0015	0.018 ± 0.018	0.003 ± 0.003
Total	$37,326 \pm 95$	24.137 ± 0.075	24.614 ± 0.123	0.477 ± 0.078
CI+MBPT		24.048	24.543	0.495

Table 6 Ground state α_n^{E1} values of few alkaline earth atoms, Yb and Hg, from different many-body methods

Method	Ca	Sr	Ba	Yb	Hg	Al^+	In^+
DF	122.90	156.83	218.88	122.21	40.95	19.514	25.734
MBPT(2)	151.70	188.98			34.98		
MBPT(3)	132.80	163.13			22.98	21.752	18.374
RPA					44.98	26.289	29.570
LCCSD					33.91	26.118	25.360
CCSD	157.03	186.98	268.19	144.59	34.98	24.299	24.246
CCSD(T)					33.95		
CCSDpT					34.07	24.26	24.11
+ Breit	156.83	186.80			34.16		
+ QED	~ 0.0	186.78			34.27		
CI+MBPT [38]						20.048	24.01
Experiment	169(17)	186(15)	268(22)	142(36)	33.91(34)		

There have also been α_n^{E1} values evaluated for the ground states of alkaline earth atoms, Al^+ , In^+ , Yb, and Hg, and of the ground and excited states involved in the clock transitions of alkaline earth ions by calculating the first-order perturbed wave functions due to the E1 operator using the DF and CC methods. In Table 6, results for the ground states of the above systems are listed from these calculations and experiments [23, 26, 30, 39]. Similarly, results for the ions are given and compared with the experimental values [22–25] in Table 7. Polarizabilities due to the E1, M1, and E2 operators in these ions and only due to the E1 operator in few alkali atoms are also determined precisely using the sum-over-states approaches by dividing electron correlation effects into three classes [8, 18, 40–42] as contributions: due to the valence correlation, due to correlations among the occupied electrons, and due to the core-valence correlation which are denoted by $\alpha_n^{O,v}$, $\alpha_n^{O,c}$, and $\alpha_n^{O,cv}$ for the corresponding operator O , respectively [18]. These values, with individual contributions, are given in Table 8.

Table 7 Evaluation of results in the clock transitions of alkaline earth ions using the DF and RCC methods and comparison with the available measured values taken from [22–25]

Method	Ca ⁺			Sr ⁺			Ba ⁺			Ra ⁺		
	4s _{1/2}	3d _{3/2}	3d _{5/2}	5s _{1/2}	4d _{3/2}	4d _{5/2}	6s _{1/2}	5d _{3/2}	5d _{5/2}	7s _{1/2}	6d _{3/2}	6d _{5/2}
DF	42.76	40.66	39.71	56.72	64.83	60.82	81.99	40.03	38.96	73.18	81.36	63.90
CCSD(T)	73.0	28.5	29.5	88.29	61.43	62.87	124.26	48.81	50.67	104.54	83.71	82.38
Experiment	70.89(15)			93.3(9)			123.88(5)					
	75.3(4)											
	72.5(19)											

Using the above static polarizabilities, the BBR shift due to the E1 operator for the clock transition $3s^2\ ^1S_0 \rightarrow 3s3p\ ^3P_0$ in Al⁺ yields $\Delta v = -0.0041$ Hz, while they are about 0.37, 0.22, 0.64, and 0.19 in Hz for the $ns \rightarrow (n-1)d_{5/2}$ clock transitions in the Ca⁺, Sr⁺, Ba⁺, and Ra⁺ ions, respectively, with n as the principal quantum number of the ground states of the respective ion.

In a similar approach to above sum-over-states approach, dynamic α_n^{E1} polarizabilities for both the ground and first two excited states are evaluated using both the linearly and circularly polarized lights in the alkali atoms [41, 42]. To illustrate magic wavelengths obtained from these calculations, the dynamic polarizabilities of the $5s$, $5p_{1/2}$, and $5p_{3/2}$ states in the Rb atom are plotted against the wavelengths of applied lights with both the linearly and left-handed circularly polarizations in Fig. 1a–d. **Magic wavelengths** for the $ns\ ^2S_{1/2} \rightarrow np\ ^2P_{1/2,3/2}$ transitions in the Rb atom due to these lights are indicted by pointing arrows at the crossings of the polarizability values of the above states.

Quadrupole Moments

Itano has reported quadrupole moments of many of the abovementioned ions and for Yb⁺ by performing MCDF calculations [32]. These values are compared with the CC and experimental results [6, 8, 36, 43] in Table 10. As was in the A_{hf} results, the MCDF results for the Θ values in the nd states of the Alkaline earth ions are also off than their respective experimental values, whereas CC methods were able to produce them more reliably. A detailed analysis to the passage of electron correlation effects and role of higher relativistic corrections for precise estimate of Θ values in the Ca⁺ metastable states is also demonstrated in Table 9. It can be noticed that correlation effects improve the results from the DF values significantly and occurrence of strong cancelations is found among the higher-order correlation effects. Though it appears that relativistic corrections are small in the determination of Θ values, their contributions, especially from the Breit interaction, are useful in order to reduce the uncertainty in the calculations. As can also be seen, some of the calculations are as par with the available measurements, and in some cases they are even better than their experimental values. For many states, experimental results are not known but the calculated values can be reliably trusted because the

Table 8 Determination of multipolar polarizabilities in the alkali atoms and alkaline earth ions using sum-over-states approaches as have been reported in [18, 40–42]

Ion	$\alpha_n^{O,v}$	$\alpha_n^{O,c}$	$\alpha_n^{O,cv}$	α_n^O	$\alpha_n^{O,v}$	$\alpha_n^{O,c}$	$\alpha_n^{O,cv}$	α_n^O			
$ns^2 S_{1/2}$ state											
α_n^{M1} result											
α_n^{E2} result	$(n-1)d^2 D_{5/2}$ state										
Ca ⁺	0.9×10^{-5}	5.0×10^{-5}	-1.4×10^{-8}	5.9×10^{-5}	-957	5.0×10^{-5}	0.0	-957			
Sr ⁺	2.8×10^{-6}	1.0×10^{-3}	-2×10^{-8}	1×10^{-3}	-208	1×10^{-3}	-2.5×10^{-7}	-208			
Ba ⁺	1.0×10^{-5}	3.5×10^{-4}	~ 0.0	3.6×10^{-6}	-72.63	3.5×10^{-4}	-1.4×10^{-5}	-71.63			
Ra ⁺	1.0×10^{-4}	6.3×10^{-3}	~ 0.0	6.4×10^{-3}	-35.23	6.3×10^{-3}	-2.7×10^{-5}	-35.23			
α_n^{E2} result											
Ca ⁺	900.64	6.15	0.0	906.79	-3,712.33	6.15	0.18	-3,706.00			
Sr ⁺	1,351.50	14.50	-1.7×10^{-8}	1,366	-1,746.74	14.50	0.24	-1,746.74			
Ba ⁺	4,184.80	48.51	-0.15	4,233.16	-1,357.03	48.51	-0.87	-1,309.39			
Ra ⁺	2,478.98	64.37	-0.11	2,543.22	-1,220.64	64.37	-0.58	-1,156.85			
Atom	$\alpha_n^{E1,v}$	$\alpha_n^{E1,c}$	$\alpha_n^{E1,cv}$	α_n^{E1}	Expt	$\alpha_n^{E1,v}$	$\alpha_n^{E1,c}$	$\alpha_n^{E1,cv}$	α_n^{E1}	$\alpha_n^{E1,c}$	α_n^{E1}
$ns^2 S_{1/2}$ state											
Li	163.8	0.22	~ 0.0	164.2	164.2(11)	126.75	0.22	~ 0.0	126.97	126.76	0.22
Na	161.48	0.9	~ 0.0	162.4	162.7(8)	360.1	0.9	~ 0.0	361.0	361.1	0.9
K	284.36	5.5	-0.13	289.8	290.58(1,42)	599.8	5.5	~ 0.0	605.0	610.8	5.5
Rb	309.46	9.1	-0.26	318.3	319.9(6,1)	801.4	9.1	~ 0.0	810.5	858.9	9.1
$np^2 P_{1/2}$ state											
$np^2 P_{3/2}$ state											

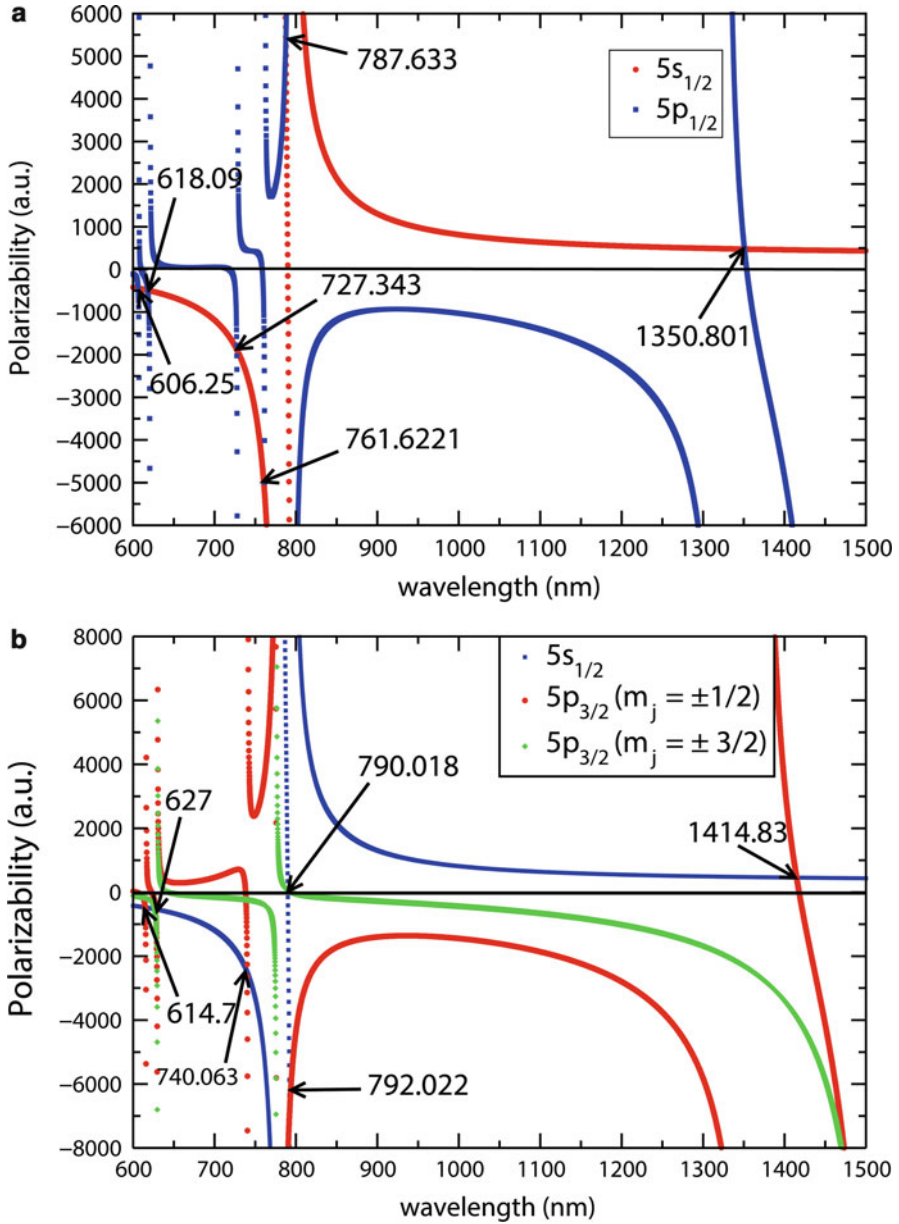


Fig. 1 Dynamic polarizabilities of the $5s$, $5p_{1/2}$, and $5p_{3/2}$ states in Rb atom corresponding to the linearly and left-handed circularly polarized lights. Magic wavelengths for (a) the $5s \rightarrow 5p_{1/2}$ transition with the linearly polarized light, (b) the $5s \rightarrow 5p_{3/2}$ transition with the linearly polarized light, (c) the $5s \rightarrow 5p_{1/2}$ transition with the circularly polarized light, and (d) the $5s \rightarrow 5p_{3/2}$ transition with the circularly polarized light, shown pointing by arrows at the crossing points

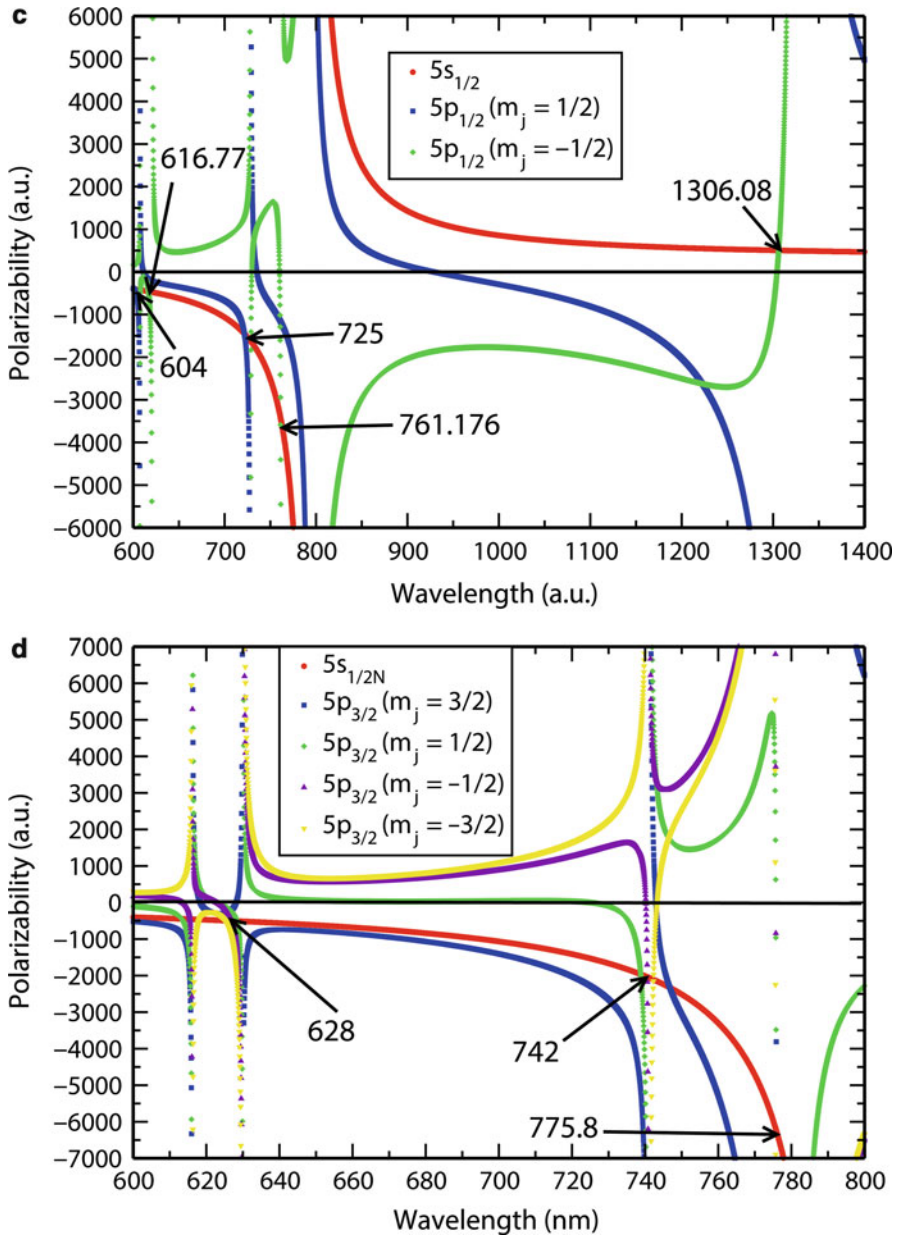


Fig. 1 (continued)

Table 9 Theoretical and experimental Θ values of states involved in the clock transitions of alkaline earth and Yb ions. A detailed analysis for the Ca^+ results given at different levels of approximations in the CC method and contributions from higher-order relativistic corrections is tabulated explicitly

Method	Ca^+		Sr^+		Ba^+		Ra^+			Yb^+	
	$3d_{3/2}$	$3d_{5/2}$	$4d_{3/2}$	$4d_{5/2}$	$5d_{3/2}$	$5d_{5/2}$	$6d_{3/2}$	$6d_{5/2}$	$5d_{3/2}$	$5d_{5/2}$	$4f_{7/2}$
DF	1.712	2.451	2.469	3.496	2.72	3.99	3.58	5.29	2.440	3.613	-0.259
MBPT(2)	1.288	1.848									
LCCSD	1.234	1.770848									
CCSD	1.309	1.877							2.068	3.116	-0.216
CCSD(T)	1.301	1.867	2.12	2.94	2.32	3.42	2.90	4.45			
CCSDvT	1.291	1.846848									
+Triples	-0.005	-0.004848									
+Breit	-0.003	-0.002848									
+QED	0.00002	0.00003848									
MCDF [32, 44]	1.338	1.917	2.107	3.048	2.297	3.379			2.174	3.244	-0.22
Experiment		1.83(1)		2.6(3)					2.08(11)		-0.041(5)

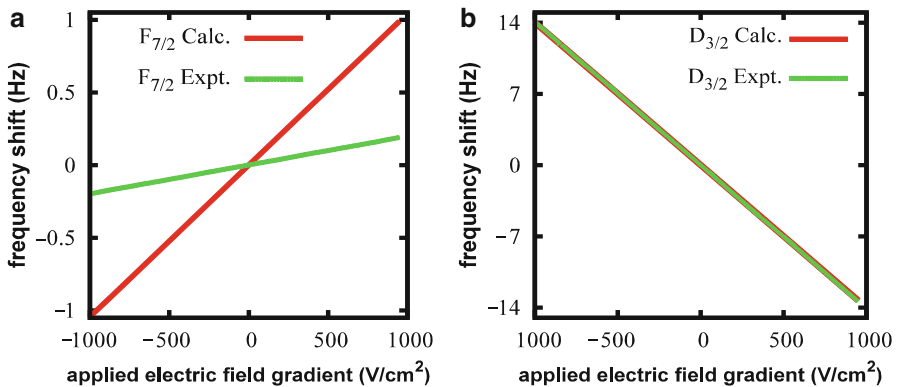


Fig. 2 Comparison between the quadrupole shifts estimated using Θ values from the measurement and calculations by the CC methods for (a) the $[4f^{14}6s]^2S_{1/2}(F=0) \rightarrow [4f^{13}6s^2]^2S_{7/2}(F=3)$ and (b) the $[4f^{14}6s]^2S_1(F=0) \rightarrow [4f^{14}5d]^2D_{3/2}(F=2)$ clock transitions in Yb^+

employed methods have been proven to give rise this quantity in other systems very accurately. In fact, it is interesting to note that calculations of Θ in the $4f_{7/2}$ state of Yb^+ using the MCDF [44] and CC [36] methods report consistent values but its corresponding experimental result is found to be quite small. This, essentially, calls for further experimental and theoretical investigation to be sure about its correct value and to scrutinize reasons for which such large discrepancies are resulting. Nevertheless, both the experimental and theoretical results for the $5d_{3/2}$ state in Yb^+ agree with each other quite nicely and uncertainty in the theoretical value is estimated to be smaller [36]. In Fig. 2, the estimated quadrupole shifts for the

clock transitions in Yb^+ using the calculated Θ values and compared with their corresponding experimental results are shown.

Clocks for Fundamental Physics

In the standard model (SM) of particle physics, there are several dimensionless “fundamental constants” such as gauge couplings whose constancies are not really predicted by the model itself, but they are accepted on some logical grounds without having sufficient scientific proof. However, this fact needs to be verified and any recognizable anomaly observed for all plausible circumstances with respect to variation in space or time that should be adequately explained by a fundamental theory. This persuades many to invent innovative notions of ideas to search for such signatures. One of the important and popular concepts is to presume dynamic behavior of some of the physical constants, which should be probed by any either direct or indirect methods [45,46]. Since all the modern atomic clocks are capable of measuring atomic transition frequencies to ultrahigh-precision level, any observed discrepancies in that place of accuracy can be interrogated. It may be suggestive not to take values of the constants directly from their single observational methods; rather, they should be extracted from a series of theoretical and experimental studies concurrently. Determination of a self-consistent set of values of the fundamental constants giving best matching between theories and a defined set of experiments can address how much constancy the physical constants are really immanent within themselves. In fact, the test of variability of the physical constants does not require knowledge of their actual values to sufficient high precision in anticipation. A procedure for inferring any possible temporal variation of α_e from the clock frequency measurements has been elucidated here.

Let a physical quantity A be decomposed as $A = k_1 F_1 = k_2 F_2$ such as both k_1 and k_2 are two dimensionless quantities, while F_1 and F_2 are two functions of the physical constants among which F_1 is a function of the base units only (say) to some power. In this case the time variation of A (denoted by dA/dt) can be given by

$$\frac{d \ln A}{dt} = \frac{d \ln k_1}{dt} + \frac{d \ln F_1}{dt} = \frac{d \ln k_2}{dt} + \frac{d \ln F_2}{dt}, \quad (66)$$

such that, let us say, time variation of either dk_1/dt or dk_2/dt can be measured for which it is mandatory to have either $dF_1/dt = 0$ or $dF_2/dt = 0$. In this condition by measuring either dk_1/dt or dk_2/dt , it is possible to infer dA/dt . This is the basic underlying principle that can be adopted to probe $d\alpha_e/dt$. The ancillary attainment from the finding of $d\alpha_e/dt$ is that this information can be used for extracting information on possible variation in quantum chromodynamics parameter Λ_{QCD} and electron (quark) mass $m_{e(q)}$ using the empirical relations [45,46]

$$\frac{\delta\Lambda_{\text{QCD}}}{\Lambda_{\text{QCD}}} \approx 34 \frac{\delta\alpha_e}{\alpha_e} \quad (67)$$

and

$$\frac{\delta m_{e(q)}}{m_{e(q)}} \approx 70 \frac{\delta\alpha_e}{\alpha_e}. \quad (68)$$

Since mass of the proton (m_p) is related with nuclear magnetic moment and is almost approximated to $m_p \approx 3\Lambda_{\text{QCD}}$, so from $d\alpha_e/dt$ along with the above two relations, variation in the ratio m_p/m_e , strong to weak scale variation, can also be determined. Any possible signature in observing variation in the above physical quantities will be very useful to support physics describing by Grand Unified Theory (GUT) and other sophisticated models of particle physics and may also imply plausible violation of Einstein's equivalence principle [45, 46].

The energy level in an atomic state of any multi-electron system is expressed as [47]

$$E_n \simeq c^2 (Z \alpha_e)^2 \left\{ \frac{1}{2n^2} + \frac{(Z \alpha_e)^2}{2n^3} \left(\frac{1}{|k_n|} - \frac{3}{4n} \right) \right\}, \quad (69)$$

where $k_n = \pm (j_n + \frac{1}{2})$ is the relativistic quantum number. Since the relativistic effects in an energy level close to the nucleus is large due to the high angular velocity of the electron and approximately given by

$$\Delta = -\frac{Z_a^2 (Z \alpha_e)^2}{2 \nu^3} \left(\frac{1}{j_n + \frac{1}{2}} - \frac{Z_a}{Z \nu} \left[1 - \frac{Z_a}{4Z} \right] \right) \quad (70)$$

where ν is the effective principal quantum number and Z_a is the effective charge experienced by the electron in that energy level after accounting the screening effects due to the inner-core electrons. As the relativistic effects in the atomic energy levels scale in the order of α_e^2 , the transition frequencies among the atomic levels are very sensitive to a small change in α_e and get enhanced with large atomic number Z and for a small value of ν . The advantage of considering atomic systems for probing variability of the physical constants is owing to the reason as any change due to a small variation in α_e in the atomic transition frequencies can be probed using the relativistic many-body methods by expressing a transition frequency (ω) as

$$\omega(x) \approx \omega_0 + q x, \quad (71)$$

where ω_0 is a referenced transition frequency with its corresponding fine-structure constant α_0 value, $x = \left(\frac{\alpha_e}{\alpha_0} \right) - 1$ is the Taylor coefficient of the first derivative of ω , and $q = \left. \frac{d\omega}{dx} \right|_{x=0}$ is known as the sensitivity coefficient due to variation in the α_e value. For the numerical estimate of the q -factor, it can be evaluated at the level of the first-order correction in α_e^2 using the expression

$$q \approx \frac{\omega(+x) - \omega(-x)}{2x} \quad (72)$$

for an arbitrary small value of x . By combining ultrahigh-precision frequencies measured in the optical frequency standards for a certain time interval with the calculated q -factors, it is possible to get some information on variation in α_e from a given reference. In the heavy atomic systems, the sensitivity parameters can be quite significant and can be of the order of one. Hence, it may be ideal to define another quantity (L_{α_e}) in the logarithmic form, to address the same issue, as

$$L_{\alpha_e} = \alpha_e \frac{\partial}{\partial \alpha_e} \ln[F_{\text{rel}}(Z\alpha_e)] \quad (73)$$

where $F_{\text{rel}}(Z\alpha_e)$ is the relativistic scaling factor in an atomic energy level. For the (optical) atomic transitions, it can be expressed as

$$L_{\alpha_e} = \frac{2q}{\omega_{\text{ref}}}, \quad (74)$$

for the reference frequency ω_{ref} .

All the microwave clocks and some of the optical clocks, by the way, involve hyperfine transitions. The magnetic-dipole hyperfine structure constant A_{hf} of an atomic state can be analytically expressed as

$$A_{\text{hf}} \propto \left[\frac{m_e e^4}{\hbar^2} \right] [\alpha_e^2 F_{\text{rel}}(Z\alpha_e)] \left[\mu_B \frac{m_e}{m_p} \right], \quad (75)$$

where for the S-wave electron $F_{\text{rel}}(Z\alpha_e) = \frac{3}{\sqrt{1-(Z\alpha_e)^2(3-(2Z\alpha_e)^2)}}$ and $L_{\alpha_e} = (Z\alpha_e)^2 \frac{11-(Z\alpha_e)^2}{(1-(Z\alpha_e)^2)(3-(2Z\alpha_e)^2)}$. It can be shown that variation in α_e is related to variation in $F_{\text{rel}}(Z\alpha_e)$ as

$$\frac{\delta F_{\text{rel}}(Z\alpha_e)}{F_{\text{rel}}(Z\alpha_e)} = K \frac{\delta \alpha_e}{\alpha_e}, \quad (76)$$

for the factor $K = \frac{(Z\alpha_e)^2}{(1-(Z\alpha_e)^2)(3-(2Z\alpha_e)^2)}$. Using this formula one obtains $K = 0.74$ for Cs, $K = 0.29$ for Rb, $K = 2.18$ for Hg^+ , etc.; however, after expressing

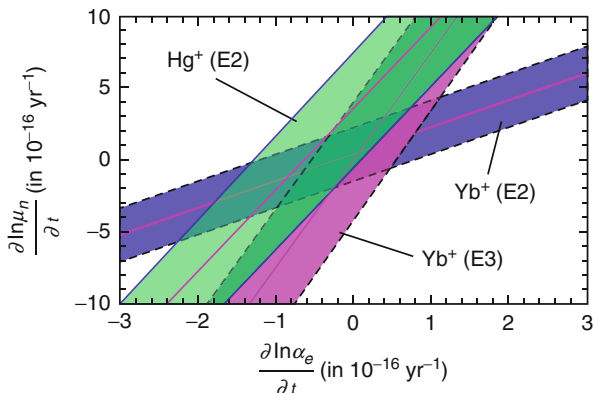
$$A_{\text{hf}} = \left(\frac{\alpha_e}{\alpha_0} \right) (A_{\text{hf}}^{\text{ref}} + qx) \quad (77)$$

for the reference $A_{\text{hf}}^{\text{ref}}$ value, it is obtained as $K = 0.83$, $K = 0.34$, and $K = 2.28$ for Cs, Rb, and Hg^+ , respectively [47].

The more straightforward relations that are convenient to use for inferring information on $d\alpha_e/dt$ from the combination of a probed transition (denoted by

Table 10 Preliminary results obtained by combining CC calculations with corresponding experimental frequency measurements from three important atomic clocks (Nandy DK, Private communication)

System	Transition	K_{rel}	$\frac{1}{R} \frac{\partial R}{\partial t}$ (in year^{-1})
Yb^+	$[4f^{14}]6s \rightarrow 5d_{3/2}$	0.951	$(0.5 \pm 1.9) \times 10^{-16}$
Yb^+	$[4f^{14}]6s \rightarrow 4f^{13}6s^2 \ ^2F_{7/2}$	-4.692	$(0.2 \pm 4.1) \times 10^{-16}$
Hg^+	$[5d^{10}]6s \rightarrow 5d^9 6s^2 \ ^2D_{5/2}$	-2.88	$(3.7 \pm 3.9) \times 10^{-16}$

Fig. 3 Constraints on temporal variations in α_e and μ_n from the quadrupole (E2) clock transitions from Yb^+ and Hg^+ ions and octopole (E3) clock transition of Yb^+ ion with reference to Cs clock using the calculated q -parameters by CC method and available experimental data

index 1) and a reference transition (referred by index 2) in the consideration of variety of transitions in an atomic system are given as [45, 46]

$$\frac{\partial}{\partial t} \ln \left[\frac{f_{\text{hfs}}^1}{f_{\text{hfs}}^2} \right] \approx \frac{\partial}{\partial t} \ln \left[\frac{\mu_I^1}{\mu_I^2} \right] + \left(\frac{\partial F_{\text{rel}}^1}{\partial \alpha_e} - \frac{\partial F_{\text{rel}}^2}{\partial \alpha_e} \right) \frac{\partial \ln \alpha_e}{\partial t}, \quad (78)$$

$$\frac{\partial}{\partial t} \ln \left[\frac{f_{\text{atm}}^1}{f_{\text{atm}}^2} \right] \approx \frac{\partial}{\partial t} \ln \left(\frac{\partial F_{\text{rel}}^1}{\partial \alpha_e} - \frac{\partial F_{\text{rel}}^2}{\partial \alpha_e} \right) \frac{\partial \ln \alpha_e}{\partial t}, \quad (79)$$

and

$$\frac{\partial}{\partial t} \ln \left[\frac{f_{\text{hfs}}^1}{f_{\text{atm}}^2} \right] \approx \frac{\partial}{\partial t} \ln \left[\frac{\mu_I^1}{\mu_I^2} + (2 + L_{\text{hfs}}^1 - L_{\text{atm}}^2) \ln \alpha_e \right], \quad (80)$$

where the abbreviations hfs and atm represent, particularly, the hyperfine and atomic transitions, respectively. At least the following quantities

$$R = \frac{f_{\text{obs}}}{f_{\text{Cs}}} \quad \text{and} \quad K_{\text{rel}} = \frac{1}{F_{\text{rel}}} \frac{\partial F_{\text{rel}}}{\partial \alpha_e}$$

for three clock transitions listed in Table 10 from the calculations using CC methods (Nandy DK, Private communication). Here Cs clock frequency standard is taken as the reference to compare with the observed values. Using these quantities,

possible variation in α_e versus variation in nuclear magnetic moment μ_n inferred from the combinations of the above three clock transitions are demonstrated pictorially in Fig. 3.

Summary

Many basic concepts on working principles, needs, and roles of theoretical studies for atomic clocks are described for the general readers. It mainly highlights the essential criterion, present status, and future prospective of atomic clocks and mentions the candidates that are capable of replacing the present Cs primary frequency standard. Optical clocks based on the neutral atoms and a single trapped singly charged ions are discussed in great detail and their constraining factors to achieve high accuracy are demonstrated by considering a few cases. Uncertainties due to both the instrumental and external fields are also briefly given. In this context, the role of relativistic many-body methods for accurate estimate of uncertainties in some of the major systematics is discussed. Underlying differences between various many-body methods that are usually employed to calculate these properties are explained and few concrete examples are shown by giving results from these methods. The importance of higher-order relativistic effects is shown by evaluating their contributions explicitly in few cases. It is seen that in several cases, the theoretical calculations are more precise than the experimental results and in some situations both the experimental and theoretical results do not match. This, obviously, calls for developing more sophisticated many-body methods to validate these results more reliably. It is also emphasized how a priori theoretical studies are acting as the guiding factors for selecting new clock candidates. Finally, the need of studying atomic clocks, both theoretically and experimentally, for probing fundamental sciences is illustrated.

Acknowledgements The author is grateful to B. P. Das, D. K. Nandy, Y. Singh, and B. Arora for many fruitful discussions. The author also thanks J. Banerji for his critical reading of the chapter. Some of the preliminary calculations were carried out using the Physical Research Laboratory HPC cluster for the demonstration purposes.

References

1. Essen L, Parry JVL (1955) An atomic standard of frequency and time interval: a caesium resonator. *Nature* 176:280–284. doi:[10.1038/176280a0](https://doi.org/10.1038/176280a0)
2. Margolis HS (2009) Optical frequency standards and clocks. *Contemp Phys* 51:37–58. doi:[10.1080/00107510903257616](https://doi.org/10.1080/00107510903257616)
3. Flambaum VV, Dzuba VA, Derevianko A (2008) Magic frequencies for cesium primary-frequency standard. *Phys Rev Lett* 101:220801-4. doi:[10.1103/PhysRevLett.101.220801](https://doi.org/10.1103/PhysRevLett.101.220801)
4. Poli N, Oates CW, Gill P, Tino GM (2013) Optical atomic clocks. *Rivista Del Nuovo Cimento* 36:555–624. doi:[10.1393/ncr/i2013-10095-x](https://doi.org/10.1393/ncr/i2013-10095-x)
5. Patrick G (2011) When should we change the definition of the second? *Philos Trans R Soc A* 369:4109–4130. doi:[10.1098/rsta.2011.0237](https://doi.org/10.1098/rsta.2011.0237)

6. Sahoo BK (2006) Relativistic coupled-cluster theory of quadrupole moments and hyperfine structure constants of 5d states in Ba⁺. *Phys Rev A* 74:020501(R)-4. doi:[10.1103/PhysRevA.74.020501](https://doi.org/10.1103/PhysRevA.74.020501)
7. Sherman JA, Trimble W, Metz S, Nagourney W, Fortson N (2005) Progress on indium and barium single ion optical frequency standards. Digest of the LEOS summer topical meetings (IEEE No. 05TH8797), e-print. arXiv:physics/0504013v2
8. Sahoo BK, Das BP, Chaudhuri R, Mukherjee D, Timmermans R, Jungmann K (2007) Investigations of Ra⁺ properties to test possibilities for new optical-frequency standards. *Phys Rev A* 76:040504(R)-4. doi:[10.1103/PhysRevA.76.040504](https://doi.org/10.1103/PhysRevA.76.040504)
9. Derevianko A, Dzuba VA, Flambaum VV (2012) Highly charged ions as a basis of optical atomic clockwork of exceptional accuracy. *Phys Rev Lett* 109:180801-180805. doi:[10.1103/PhysRevLett.109.180801](https://doi.org/10.1103/PhysRevLett.109.180801)
10. Yudin VI, Taichenachev, Derevianko A (2014) Magnetic-dipole transitions in highly charged ions as a basis of ultraprecise optical clocks. *Phys Rev Lett* 113:233003-5. doi:[10.1103/PhysRevLett.113.233003](https://doi.org/10.1103/PhysRevLett.113.233003)
11. Peik E, Tamm Chr (2003) Nuclear laser spectroscopy of the 3.5 eV transition in Th-229. *Europhys Lett* 61:181–186. doi:[10.1209/epl/i2003-00210-x](https://doi.org/10.1209/epl/i2003-00210-x)
12. Campbell CJ, Radnaev AG, Kuzmich A, Dzuba VA, Flambaum VV, Derevianko A (2012) Single-ion nuclear clock for metrology at the 19th decimal place. *Phys Rev Lett* 108:120802-5. doi:[10.1103/PhysRevLett.108.120802](https://doi.org/10.1103/PhysRevLett.108.120802)
13. Schiller S, Bakalov D, Korobov VI (2014) Simplest molecules as candidates for precise optical clocks. *Phys Rev Lett* 113:023004-5. doi:[10.1103/PhysRevLett.113.023004](https://doi.org/10.1103/PhysRevLett.113.023004)
14. Karr J-Ph (2014) H₂⁺ and HD⁺: candidates for a molecular clock. *J Mol Spectrosc* 300:37–43. doi:[10.1016/j.jms.2014.03.016](https://doi.org/10.1016/j.jms.2014.03.016)
15. Akhiezer AJ, Berestetskii VB (1965) *Quantum electrodynamics*. Interscience, New York. Chap 8, Sec 20
16. Lindroth E, Ynnerman A (1993) Ab initio calculations of g_J factors for Li, Be⁺, and Ba⁺. *Phys Rev A* 47:961–970. doi:[10.1103/PhysRevA.47.961](https://doi.org/10.1103/PhysRevA.47.961)
17. Porsev SG, Derevianko A (2006) Multipolar theory of blackbody radiation shift of atomic energy levels and its implications for optical lattice clocks. *Phys Rev A* 74:020502-4. doi:[10.1103/PhysRevA.74.020502](https://doi.org/10.1103/PhysRevA.74.020502)
18. Arora B, Nandy DK, Sahoo BK (2012) Multipolar blackbody radiation shifts for single-ion clocks. *Phys Rev A* 85:012506-10. doi:[10.1103/PhysRevA.85.012506](https://doi.org/10.1103/PhysRevA.85.012506)
19. Flambaum VV, Ginges JSM (2005) Radiative potential and calculations of QED radiative corrections to energy levels and electromagnetic amplitudes in many-electron atoms. *Phys Rev A* 72:052115-13. doi:[10.1103/PhysRevA.72.052115](https://doi.org/10.1103/PhysRevA.72.052115)
20. Shavitt I, Bartlett RJ (2009) *Many-body methods in chemistry and physics*. Cambridge University Press, Cambridge
21. Kállay M, Nataraj HS, Sahoo BK, Das BP, Visscher L (2011) Relativistic general-order coupled-cluster method for high-precision calculations: Application to the Al⁺ atomic clock. *Phys Rev A* 83:030503-4(R). doi:[10.1103/PhysRevA.83.030503](https://doi.org/10.1103/PhysRevA.83.030503)
22. Sahoo BK (2008) An ab initio relativistic coupled-cluster theory of dipole and quadrupole polarizabilities: applications to a few alkali atoms and alkaline earth ions. *Chem Phys Lett* 448:144–149. doi:[10.1016/j.cplett.2007.09.079](https://doi.org/10.1016/j.cplett.2007.09.079)
23. Sahoo BK, Das BP (2008) Relativistic coupled-cluster studies of dipole polarizabilities in closed-shell atoms. *Phys Rev A* 77:062516-5. doi:[10.1103/PhysRevA.77.062516](https://doi.org/10.1103/PhysRevA.77.062516)
24. Sahoo BK, Das BP, Mukherjee D (2009) Relativistic coupled-cluster studies of ionization potentials, lifetimes, and polarizabilities in singly ionized calcium. *Phys Rev A* 79:052511-9. doi:[10.1103/PhysRevA.79.052511](https://doi.org/10.1103/PhysRevA.79.052511)
25. Sahoo BK, Timmermans RGE, Das BP, Mukherjee D (2009) Comparative studies of dipole polarizabilities in Sr⁺, Ba⁺, and Ra⁺ and their applications to optical clocks. *Phys Rev A* 80:062506-10. doi:[10.1103/PhysRevA.80.062506](https://doi.org/10.1103/PhysRevA.80.062506)
26. Singh Y, Sahoo BK, Das BP (2013) Correlation trends in the ground-state static electric dipole polarizabilities of closed-shell atoms and ions. *Phys Rev A* 88:062504-11. doi:[10.1103/PhysRevA.88.062504](https://doi.org/10.1103/PhysRevA.88.062504)

27. Dalgarno A (1962) Atomic polarizabilities and shielding factors. *Adv Phys* 11:281–315. doi:[10.1080/00018736200101302](https://doi.org/10.1080/00018736200101302)
28. Szabo A, Ostlund NS (1989) *Modern quantum chemistry*. Dover, New York
29. Peng D, Ma J, Liu W (2009) *Int J Quantum Chem* 109:2149–2167. doi:[10.1002/qua.22078](https://doi.org/10.1002/qua.22078)
30. Singh Y, Sahoo BK (2015) Rigorous limits on the hadronic and semileptonic CP-violating coupling constants from the electric dipole moment of Hg199. *Phys Rev A* 91, 030501-5. doi:[10.1103/PhysRevA.91.030501](https://doi.org/10.1103/PhysRevA.91.030501)
31. Nandy DK, Singh Y, Sahoo BK (2013) Development of a relativistic coupled-cluster method for one-electron detachment theory: application to Mn ix, Fe x, Co xi, and Ni xii ions. *Phys Rev A* 88:052512-12. doi:[10.1103/PhysRevA.88.052512](https://doi.org/10.1103/PhysRevA.88.052512)
32. Itano WM (2005) Quadrupole moments and hyperfine constants of metastable states of Ca+, Sr+, Ba+, Yb+, Hg+, and Au. *Phys Rev A* 73:022510-11. doi:[10.1103/PhysRevA.73.022510](https://doi.org/10.1103/PhysRevA.73.022510)
33. Sahoo BK, Sur C, Beier T, Das BP, Chaudhuri RK, Mukherjee D (2007) Enhanced role of electron correlation in the hyperfine interactions in D5/22 states in alkaline-earth-metal ions. *Phys Rev A* 75:042504-6. doi:[10.1103/PhysRevA.75.042504](https://doi.org/10.1103/PhysRevA.75.042504)
34. Sahoo BK, Das BP (2011) Parity nonconservation in ytterbium ion. *Phys Rev A* 84:010502-4(R). doi:[10.1103/PhysRevA.84.010502](https://doi.org/10.1103/PhysRevA.84.010502)
35. Versolato OO, Giri GS, Wansbeek LW, van den Berg JE, van der Hoek DJ, Jungmann K, Kruihof WL, Onderwater CJG, Sahoo BK, Santra B, Shidling PD, Timmermans RGE, Willmann L, Wilschut HW (2010) Laser spectroscopy of trapped short-lived Ra+ ions. *Phys Rev A* 82:010501-4. doi:[10.1103/PhysRevA.82.010501](https://doi.org/10.1103/PhysRevA.82.010501)
36. Nandy DK, Sahoo BK (2014) Quadrupole shifts for the Yb+171 ion clocks: Experiments versus theories. *Phys Rev A* 90:050503-5(R). doi:[10.1103/PhysRevA.90.050503](https://doi.org/10.1103/PhysRevA.90.050503)
37. Tommaseo G, Pfeil T, Revalde G, Werth G, Indelicato P, Desclaux JP (2003) The gJ-factor in the ground state of Ca+. *Eur Phys J D* 25:113–121. doi:[10.1140/epjd/e2003-00096-6](https://doi.org/10.1140/epjd/e2003-00096-6)
38. Safronova MS, Kozlov MG, Clark CW (2012) Precision calculation of blackbody radiation shifts for optical frequency metrology. *Phys Rev Lett* 107:143006-5. doi:[10.1103/PhysRevLett.107.143006](https://doi.org/10.1103/PhysRevLett.107.143006)
39. Singh Y, Sahoo BK (2014) Correlation trends in the polarizabilities of atoms and ions in the boron, carbon, and zinc homologous sequences of elements. *Phys Rev A* 90:022511-8. doi:[10.1103/PhysRevA.90.022511](https://doi.org/10.1103/PhysRevA.90.022511)
40. Sahoo BK (2014) Role of the multipolar black-body radiation shifts in the atomic clocks at the 10–18 uncertainty level. *Pramana* 83:255–263. doi:[10.1007/s12043-014-0791-9](https://doi.org/10.1007/s12043-014-0791-9)
41. Arora A, Sahoo BK (2012) State-insensitive trapping of Rb atoms: linearly versus circularly polarized light. *Phys Rev A* 86:033416-12. doi:[10.1103/PhysRevA.86.033416](https://doi.org/10.1103/PhysRevA.86.033416)
42. Sahoo BK, Arora B (2013) Magic wavelengths for trapping the alkali-metal atoms with circularly polarized light. *Phys Rev A* 87:023402-9. doi:[10.1103/PhysRevA.87.023402](https://doi.org/10.1103/PhysRevA.87.023402)
43. Sur C, Latha KVP, Sahoo BK, Chaudhuri RK, Das BP, Mukherjee D (2006) Electric quadrupole moments of the D states of alkaline-earth-metal ions. *Phys Rev Lett* 96:193001-4. doi:[10.1103/PhysRevLett.96.193001](https://doi.org/10.1103/PhysRevLett.96.193001)
44. Blythe PJ, Webster SA, Hosaka K, Gill P (2003) Systematic frequency shifts of the 467 nm electric octupole transition in 171Yb+. *J Phys B: At Mol Opt Phys.* 36:981–989. doi:[10.1088/0953-4075/36/5/317](https://doi.org/10.1088/0953-4075/36/5/317)
45. Uzan J-P (2003) The fundamental constants and their variation: observational and theoretical status. *Rev Mod Phys* 75:403–455. doi:[10.1103/RevModPhys.75.403](https://doi.org/10.1103/RevModPhys.75.403)
46. Kolachevsky NK (2004) Laboratory search for time variation in the fine structure constant. *Phys-Usp* 47:1101–1108. doi:[10.1070/PU2004v047n11ABEH001870](https://doi.org/10.1070/PU2004v047n11ABEH001870)
47. Dzuba VA, Flambaum VV, Webb JK (1999) Calculations of the relativistic effects in many-electron atoms and space-time variation of fundamental constants. *Phys Rev A* 59:230–237. doi:[10.1103/PhysRevA.59.230](https://doi.org/10.1103/PhysRevA.59.230)